

TWICE IS ENOUGH FOR DANGEROUS EIGENVALUES*

ANDREW HORNING[†] AND YUJI NAKATSUKASA[‡]

Abstract. We analyze the stability of a class of eigensolvers that target interior eigenvalues with rational filters. We show that subspace iteration with a rational filter is stable even when an eigenvalue is located near a pole of the filter. These dangerous eigenvalues contribute to large round-off errors in the first iteration, but are self-correcting in later iterations. In contrast, Krylov methods accelerated by rational filters with fixed poles typically fail to converge to unit round-off accuracy when an eigenvalue is close to a pole. In the context of Arnoldi with shift-and-invert enhancement, we demonstrate a simple restart strategy that recovers full precision in the target eigenpairs.

Key words. subspace iteration, Arnoldi, shift-and-invert, rational filters, contour integral eigen-solvers, FEAST

AMS subject classifications.

1. Introduction. Subspace iteration and Arnoldi with shift-and-invert enhancement are two classic iterative schemes for computing a few interior eigenvalues of an $n \times n$ matrix A . Each method constructs an orthonormal basis for a search subspace by iteratively applying the spectral filter

$$(1.1) \quad s(A) = (zI - A)^{-1}$$

to a set of vectors. Approximate eigenpairs can then be extracted from the search subspace with a projection step, e.g., Rayleigh–Ritz. The shift z is selected to target a region of interest and both methods typically approximate eigenvalues of A closest to z .

Recently, general rational filters of the form

$$(1.2) \quad r(A) = \sum_{j=1}^{\ell} \omega_j (z_j I - A)^{-1}.$$

have attracted a great deal of attention in the context of large, data-sparse eigenvalue problems [1, 4, 6, 8, 11, 14]. When the weights $\omega_1, \dots, \omega_\ell$ and nodes z_1, \dots, z_ℓ are chosen appropriately, these rational filters can robustly target eigenvalues in a region of interest and significantly accelerate convergence of the subspaces constructed by subspace iteration, Arnoldi, or variants thereof [1, 14]. They also tend to be highly parallelizable because each shift-and-invert transformation may be applied independently [6].

In his 2001 volume on matrix algorithms for eigenvalue problems, Stewart noted that shift-and-invert Arnoldi encounters difficulties in floating point arithmetic when the shift lies too close to an eigenvalue of A [12, p. 309]. Although the eigenvalue adjacent to the shift is rapidly approximated to the order of the unit round-off u , the residuals of other computed eigenpairs stagnate near the order of u/d , where d is the distance between the “dangerous” eigenvalue and the shift. This phenomenon has also recently been observed in the context of Krylov methods where the subspace is constructed with contour integrals and rational approximation [1].

*Submitted to the editors March 26, 2022.

Funding: The work of the first author was partially support by NSF DMS-1818757.

[†]Center for Applied Mathematics, Cornell University, Ithaca, NY 14853. (ajh326@cornell.edu)

[‡]Mathematical Institute, University of Oxford, Oxford, OX2 6GG. (nakatsukasa@maths.ox.ac.uk)

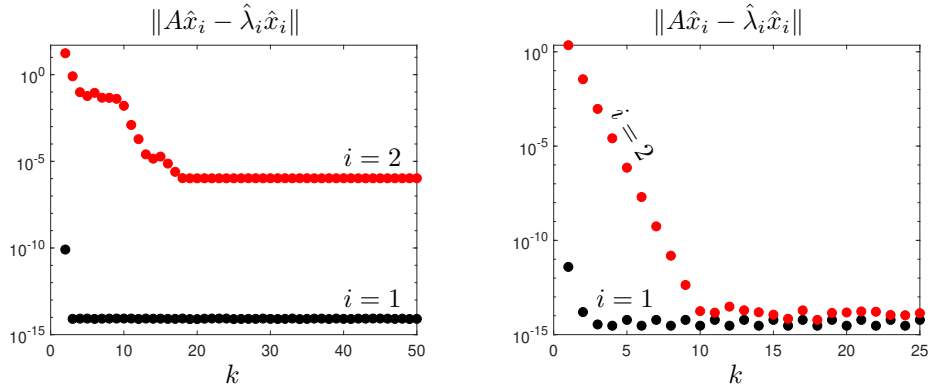


FIGURE 1.1. The residuals for two approximate eigenpairs of a real-symmetric 100×100 matrix at iterations $k = 2, \dots, 50$ of Arnoldi (left) and iterations $k = 1, \dots, 25$ of subspace iteration (right), both with shift-and-invert enhancement. The approximate eigenpairs correspond to a dangerous eigenvalue (black) with $|z - \lambda_1| = 10^{-12}$ and a second target eigenvalue (red) with $|z - \lambda_2| \approx 0.1$.

Curiously, dangerous eigenvalues do not inflict the same stagnation in the residuals of the other target eigenpairs during subspace iteration. Figure 1.1 compares the residuals of two target eigenpairs computed with Arnoldi (left) and subspace iteration (right), using the shift-and-invert filter in (1.1) with $z = 10$. The approximation to the dangerous eigenvalue $\lambda_1 = 10 + 10^{-12}$ converges rapidly to unit round-off accuracy in both cases. However, only subspace iteration computes an approximation to the second target eigenvalue $\lambda_2 \approx 10.1$ to unit round-off accuracy.

A similar story unfolds in Figure 1.2, where we compute two target eigenpairs with the contour integral eigensolver described in [14], one of them located at distance 10^{-10} from the contour. As we refine the quadrature along the contour, the poles of a rational filter with form (1.2) cluster near the dangerous eigenvalue and we observe the residual of the dangerous eigenpair converge rapidly to unit round-off, while the residuals of the remaining target pairs stagnate near 10^{-5} . On the other hand, if we fix the number of quadrature points (i.e., poles) and refine via filtered subspace iteration, the residuals of all target eigenpairs converge geometrically to order u .

This paper is about explaining Figures 1.1 and 1.2. We first examine how rational filtered subspace iteration disarms dangerous eigenvalues after the first iteration. When A has a complete set of orthonormal eigenvectors, orthogonal bases for the search subspace play a special role and “twice-is-enough” to recover full precision in the computed iterates (see sections 3 to 5).¹ In the non-normal case, iterating on approximate eigenvectors (obtained from a Rayleigh–Ritz step, for instance) is the key to overcoming round-off errors incurred by the dangerous eigenvalue, while iterations based on orthogonal bases (such as approximate Schur vectors) suffer stagnation in the remaining target eigenpairs (see section 6).

To obtain full precision in the remaining target eigenpairs for Arnoldi and related Krylov schemes, the prevailing consensus is to alter the rational filter by moving or removing the offending poles [1, 12]. Unfortunately, this usually means settling for a less efficient filter or starting over with a new filter. Informed by our analysis of subspace iteration and its immunity to dangerous eigenvalues, we offer simple restart strategies that fix stagnation in shift-and-invert Arnoldi (see section 7).

¹Aspects of our analysis are in a spirit similar to Parlett and Kahan’s “twice-is-enough” algorithm and analysis for Gram–Schmidt reorthogonalization [7, pp.107–109].

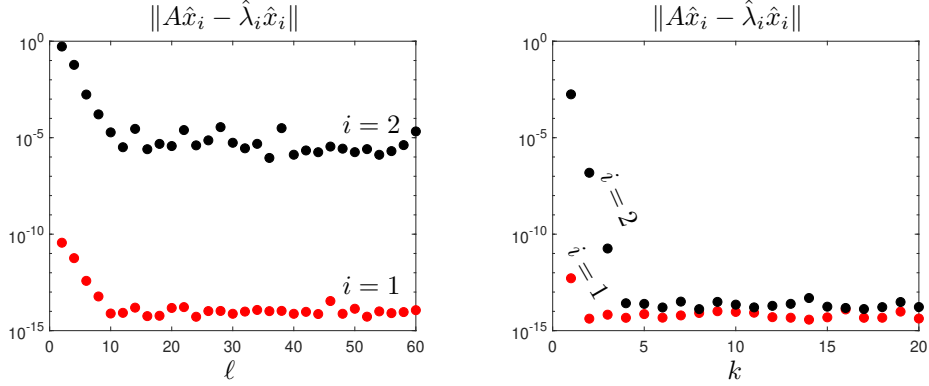


FIGURE 1.2. The left panel displays the residuals for two approximate eigenpairs of a 100×100 real-symmetric matrix computed with the contour integral eigensolver described in [14], as the quadrature rule approximating the contour integral is refined. One of the target eigenvalues ($i = 1$, black) is a distance of 10^{-10} from the contour. The right panel displays the residuals for the two approximate eigenpairs when refined via iteration rather than quadrature rule. The quadrature rule used here corresponds to a rational filter in (1.2) with $\ell = 8$.

Our analysis focuses on the situation where A has a single dangerous eigenvalue located at a distance $d \ll 1$ from a pole of the filter in (1.2). To reveal the precise influence of the dangerous eigenvalue, we frame our discussion in the asymptotic limit $d \rightarrow 0$. However, we always provide leading order estimates or concrete bounds to elucidate interaction between the dangerous eigenvalue and other practical parameters. We consider the implications of our results for other natural configurations, such as clusters of eigenvalues at a single pole and clusters at multiple poles, in section 8.

Throughout the manuscript, A denotes an $n \times n$ matrix with eigenvalues and eigenvectors satisfying $Av_i = \lambda_i v_i$, for $1 \leq i \leq n$. Except in section 6, we assume that A has a complete orthonormal set of eigenvectors, in which case it is convenient to write the eigendecomposition of A in the form

$$(1.3) \quad A = V_1 \Lambda_1 V_1^* + V_2 \Lambda_2 V_2^*.$$

Here, $\Lambda_1 = \text{diag}(\lambda_1, \dots, \lambda_m)$ contains a set of target eigenvalues that we wish to compute and $\Lambda_2 = \text{diag}(\lambda_{m+1}, \dots, \lambda_n)$ contains the remaining unwanted eigenvalues (usually, $m \ll n$). We denote the target eigenspace by $\mathcal{V} = \text{span}(V_1)$ and the full spectrum of A by $\Lambda = \Lambda_1 \cup \Lambda_2$. For simplicity, we always assume that $r(\Lambda)$ is invertible, that there is a nonzero spectral gap between $r(\Lambda_1)$ and $r(\Lambda_2)$, and index the eigenvalues in order of decreasing modulus under the filter, so that

$$(1.4) \quad |r(\lambda_1)| \geq \dots \geq |r(\lambda_m)| > |r(\lambda_{m+1})| \geq \dots \geq |r(\lambda_n)|.$$

Here, $r(\lambda) = \sum_{j=1}^{\ell} w_j (z_j - \lambda)^{-1}$ is the scalar form of the filter in (1.2).² Under the ordering in (1.4), the dangerous eigenvalue is λ_1 . Without loss of generality, we assume that the weight w_j associated with pole near the dangerous eigenvalue λ_1 is equal to one (by scaling $r(\cdot)$ if necessary).

2. Subspace iteration with rational filters. Given an $n \times m$ matrix Q_0 with orthonormal columns, the simplest practical form of subspace iteration with a rational

²We refer to the scalar function $r(z)$ and its matrix companion $r(A)$ with the same symbol. We always include the argument when it is necessary to clarify which we mean.

filter, as in (1.2), computes the iterates

$$(2.1) \quad X_k = r(A)Q_{k-1}, \quad Q_k = \text{qf}(X_k).$$

Here, $\text{qf}(X_k)$ denotes the orthogonal factor from a QR decomposition of X_k . The eigenvalues of $Q_k^*AQ_k$ provide approximations to the target eigenvalues and approximate eigenvectors are given by $Q_k x_i$ for each eigenvector, x_i , of $Q_k^*AQ_k$. These approximations to the target eigenpairs are called Ritz pairs.

Intuitively, the Ritz pairs extracted with the basis Q_k are usually good approximations to the target eigenpairs when there are good approximations to v_1, \dots, v_m in $\mathcal{S}_k = \text{span}(Q_k)$. Here, the rational filter in (2.1) fills two complimentary roles. First, the filter should guide the iterates toward the target eigenspace by mapping the target eigenvalues of A to the dominant eigenvalues of $r(A)$ (that is, the eigenvalues with largest modulus $|r(\lambda_i)|$). Second, the filter should enhance the gap between the target eigenvalues and the unwanted eigenvalues in order to accelerate the convergence of the Ritz pairs. These criteria follow from a standard one-step refinement bound for subspace iteration [9, Thm. 5.2].

THEOREM 2.1. *Let $A \in \mathbb{C}^{n \times n}$ and $r : \Lambda \rightarrow \mathbb{C}$ satisfy (1.3) and (1.4), respectively, and let $\mathcal{S}_j = \text{span}(Q_j)$ in (2.1), for $j = k-1, k$. If $V_1^*Q_{k-1}$ has full rank, then for each $v_i \in \mathcal{V}$ there are vectors $s_i^{(j)} \in \mathcal{S}_j$ such that*

$$(2.2) \quad \|s_i^{(k)} - v_i\| \leq \left| \frac{r(\lambda_{m+1})}{r(\lambda_i)} \right| \|s_i^{(k-1)} - v_i\|.$$

Moreover, $P_{\mathcal{V}}s_i^{(j)} = v_i$, where $P_{\mathcal{V}} = V_1V_1^*$ is the spectral projector onto \mathcal{V} .

Theorem 2.1 implies that there are approximations in \mathcal{S}_k that converge geometrically to the i th target eigenvector with rate $|r(\lambda_{m+1})|/|r(\lambda_i)|$.³ Consequently, if the filter is very small on the unwanted eigenvalues relative to its magnitude on the target eigenvalues, then we expect the Ritz pairs to converge rapidly. The appeal of rational filters in the modern computing era is that filters of modest degree $\ell \leq 20$ often achieve $|r(\lambda_{m+1})|/|r(\lambda_m)| \approx u$. In a typical parallel computing environment, the individual shifted inverses in (1.2) are easily applied in parallel, meaning that the target eigenpairs can be computed to machine precision at the equivalent (serial) cost of solving a shifted linear system! Of course, difficulties also arise. For example, a higher degree rational filter and multiple iterations may be required when many eigenvalues are clustered near the target group. Additionally, clustered eigenvalues may lead to ill-conditioned eigenvectors and loss of orthogonality in the Ritz pairs. In the vein of this manuscript, when eigenvalues are clustered and more poles are employed in the rational filter, one may also encounter dangerous eigenvalues.

In practice, there are many modifications one can make to (2.1) to improve convergence, fortify stability, or increase computational efficiency. However, when A has a complete set of orthogonal eigenvectors, (2.1) is enough to capture both the dangers and the disarmament of eigenvalues that are close to the poles in (1.2). When A is non-normal, iterations that incorporate the Ritz vectors when forming Q_{k-1} play a special role, while other variants (including (2.1) itself) typically fail to converge to full precision, as in Figure 1.1. We discuss these modifications further in section 6.

³If A does not possess orthogonal eigenvectors, this geometric convergence rate is only asymptotic as $k \rightarrow \infty$ due to the phenomena of transient growth in matrix powers of non-normal matrices [16, Ch. 16].

2.1. Principle angles between subspaces. The principle angles between the subspaces \mathcal{S}_k and \mathcal{V} provide a natural framework with which to characterize the refinement of the iterates in (2.1). Generalizing the notion of an angle between two vectors, the principle angles tell us how close \mathcal{S}_k and \mathcal{V} are in a geometric sense [2].

DEFINITION 2.2. Let \mathcal{X} and \mathcal{Y} be two m -dimensional subspaces with orthonormal bases X and Y , respectively, and let $\sigma_i(Y^*X)$ denote the i th singular value of Y^*X . The principle angles between \mathcal{X} and \mathcal{Y} are the acute angles $\theta_1(\mathcal{X}, \mathcal{Y}) \geq \dots \geq \theta_m(\mathcal{X}, \mathcal{Y})$ satisfying

$$(2.3) \quad \cos \theta_i(\mathcal{X}, \mathcal{Y}) = \sigma_{m+1-i}(Y^*X), \quad i = 1, \dots, m.$$

The sine of the largest principle angle, given by $\sin \theta_1(\mathcal{X}, \mathcal{Y}) = \|(I - P_{\mathcal{Y}})X\|$, defines a metric on the set of m -dimensional subspaces. However, the tangents of the principle angles, which are the singular values of the matrix [18]

$$(2.4) \quad T(X, Y) = (I - P_{\mathcal{Y}})X(Y^*X)^+,$$

are better equipped to describe the behavior of the iterates in (2.1). In (2.4), $(Y^*X)^+$ denotes the Moore-Penrose pseudoinverse of Y^*X and, crucially, X need not be orthonormal.

A subspace analogue of [Theorem 2.1](#), based on the largest principle angle between \mathcal{S}_k and \mathcal{V} , is easy to derive with (2.4). We note that [Theorem 2.1](#) is recovered from (2.6) by post-multiplying each side by the unit vector e_i and setting $s_j = X_k(V_1^*X_k)^+e_i$, for $j = k - 1, k$.

THEOREM 2.3. Let $A \in \mathbb{C}^{n \times n}$ and $r : \Lambda \rightarrow \mathbb{C}$ satisfy (1.3) and (1.4), respectively. If $\cos \theta_1(\mathcal{S}_0, \mathcal{V}) > 0$, then

$$(2.5) \quad \tan \theta_1(\mathcal{S}_k, \mathcal{V}) \leq \left| \frac{r(\lambda_{m+1})}{r(\lambda_m)} \right| \tan \theta_1(\mathcal{S}_{k-1}, \mathcal{V}) \leq \left| \frac{r(\lambda_{m+1})}{r(\lambda_m)} \right|^k \tan \theta_1(\mathcal{S}_0, \mathcal{V}).$$

Proof. We prove the first inequality with a direct calculation using (2.4); the second follows immediately by induction and the fact that $\cos \theta > 0$ when $\tan \theta < \infty$. We compute that $(I - P_{\mathcal{V}})X_k = V_2r(\Lambda_2)V_2^*Q_{k-1}$ and that $V_1^*X_k = r(\Lambda_1)V_1^*Q_{k-1}$. Using the hypothesis that $\cos \theta_1(\mathcal{S}_{k-1}, \mathcal{V}) > 0$, which implies $V_1^*Q_{k-1}$ is invertible, we obtain

$$(2.6) \quad (I - P_{\mathcal{V}})X_k(V_1^*X_k)^+ = V_2r(\Lambda_2)V_2^*Q_{k-1}(V_1^*Q_{k-1})^{-1}r(\Lambda_1)^{-1}.$$

The theorem follows by taking norms and noting that $\|V_2^*Q_{k-1}(V_1^*Q_{k-1})^{-1}\| = \tan \theta_1(\mathcal{S}_{k-1}, \mathcal{V})$, $\|r(\Lambda_2)\| = |r(\lambda_{m+1})|$, and $\|r(\Lambda_1)^{-1}\| = |r(\lambda_m)|^{-1}$. \square

The tangents (and sines) of the principle angles play an important role in the perturbation theory of eigenpairs and, consequently, the bounds in [Theorem 2.3](#) are useful when determining the accuracy in the computed Ritz pairs [9, 12, 13]. For our purposes, [Theorem 2.3](#) and its proof are useful tools when analyzing subspace iterations subject to perturbations (see [section 5](#)), because $\tan \theta_1(\mathcal{S}_k, \mathcal{V})$ is computed directly from the iterate X_k .

3. Dangerous eigenvalues. When an eigenvalue of A is very close to a pole of the rational filter in (1.2), $r(A)$ disproportionately amplifies components in the direction of the associated eigenvector. Given any vector $x \in \mathbb{C}^n$, we estimate

$$(3.1) \quad r(A)x = \sum_{i=1}^n r(\lambda_i)v_i v_i^*x = \frac{v_1^*x}{d}v_1 + \mathcal{O}(1), \quad \text{as } d \rightarrow 0.$$

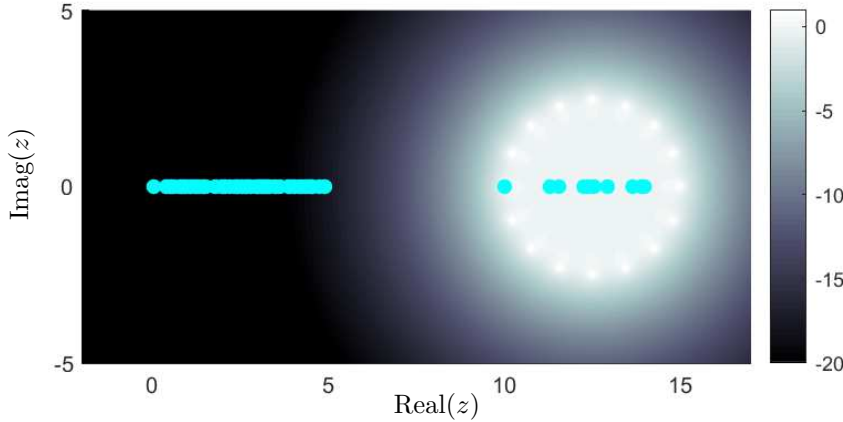


FIGURE 3.1. The eigenvalues of a 100×100 real-symmetric matrix overlaid on a complex color plot of the magnitude of a rational approximation to the characteristic function on $[10, 15]$. A dangerous eigenvalue is located at distance $d = 10^{-10}$ from the pole at $z = 10$.

This amplification is precisely the reason that shift-and-invert power iterations are so effective when the shift is close to the target eigenvalue. If we apply $r(A)$ to a random vector with unit norm and normalize, the result approximates v_1 with relative accuracy $\mathcal{O}(d)$, provided that the random vector is not nearly orthogonal to v_1 . Similarly, when $r(A)$ is applied to a random orthonormal matrix Q_0 , $\text{span}(r(A)Q_0)$ contains good approximations to v_1 if $V_1^*Q_0$ is well-conditioned.

However, the amplifying effect of a dangerous eigenvalue may cause issues when computing the iterates in (2.1) in floating point arithmetic. Figure 3.1 shows the eigenvalues of a 100×100 real symmetric matrix plotted in the complex plane over the magnitude (indicated by color) of a rational filter targeting the interval $[10, 15]$. The matrix has a large cluster of eigenvalues in the interval $[0, 5]$, where the filter has decayed to less than unit round-off, and a small set of eigenvalues in the target region, where the filter has magnitude close to 1. One eigenvalue of the matrix is very close to the pole at $z = 10$, separated by a distance of 10^{-10} . By Theorem 2.1, we expect that (in exact arithmetic) all of the eigenvalues in the target region are resolved to accuracy on the order of u after one iteration. However, Figure 3.2 (left) shows that only the dangerous eigenpair has been computed accurately. The residuals of the remaining target eigenpairs are on the order of 10^{-5} , that is, roughly u/d .

The large residuals are best explained with a look at the computed orthonormal basis \hat{Q}_1 in the eigenvector coordinates in Figure 3.2. The first column of \hat{Q}_1 (circular markers) looks as expected: the dangerous eigenvector dominates and the unwanted components are near the unit round-off in magnitude. However, the magnitude of the unwanted components is much larger, on the order of u/d , in the remaining columns $\hat{q}_2^{(1)}, \dots, \hat{q}_m^{(1)}$. The 10th column (triangular markers in Figure 3.2) is representative of this observation. Although the quality of the filter means that the unwanted components should be on the order of u in the columns of \hat{Q}_1 , they are polluted with noise on the order of u/d in all but the first column. Consequently, the accuracy in the remaining Ritz pairs computed from \hat{Q}_1 is also degraded to u/d .

There are two potential sources of error degrading the accuracy in \hat{Q}_1 . The first is the most obvious: round-off errors are amplified when solving the ill-conditioned linear system associated with the dangerous eigenvalue. The second source, more

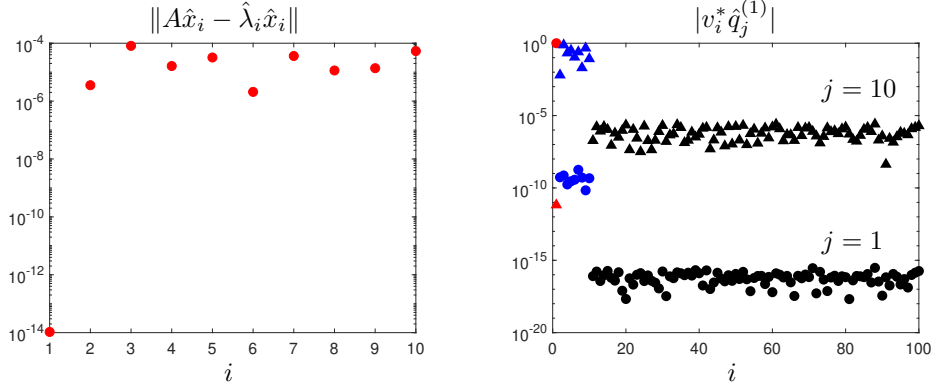


FIGURE 3.2. The residuals of 10 target eigenpairs of a 100×100 real-symmetric matrix after one iteration of subspace iteration with the rational filter in Figure 3.1 are plotted on the left. On the right are the eigenvector coordinates of the 1st (circles) and 10th (triangles) columns of Q_1 . The dangerous component (red) and the remaining target components (blue) dominate in columns 1 and 10, respectively. The unwanted eigenvector components (black) are filtered out almost perfectly to order u in the 1st column, but are orders of magnitude larger in the 10th column, with magnitude near u/d .

subtle, is the overwhelming dominance of the dangerous eigenvector in each column of X_1 , leading to an ill-conditioned basis for \mathcal{S}_1 . Remarkably, the heart of the story in Figures 1.1 and 1.2 is contained in the latter, subtler effect and we can learn a great deal without mentioning errors incurred while applying $r(A)$. Of course, a thorough understanding requires a careful treatment of the ill-conditioned linear systems and the accumulation of errors at each iteration. We address both points in section 5, where we study the convergence and stability of the iteration in (2.1) when computed in floating point arithmetic. For now, we focus on the influence of ill-conditioning in the iterates X_1, X_2, \dots , noting that round-off errors in the computed iterates have little effect on their condition number (see section 5 for a full explanation).

3.1. Accuracy of the computed orthonormal basis. When a basis $X \in \mathbb{C}^{n \times m}$ is ill-conditioned, small perturbations to the columns can have a large effect on their span. This is reflected in the sensitivity of the orthogonal factor in the QR factorization, $Q = \text{qf}(X)$. If, for some $\epsilon > 0$, X is perturbed by ΔX with $\|\Delta X\| \leq \epsilon \|X\|$, then there is a ΔQ such that $Q + \Delta Q = \text{qf}(X + \Delta X)$ and [5, p.382]

$$(3.2) \quad \|\Delta Q\| \leq c_m \kappa(X) \|\Delta X\| / \|X\|.$$

Here, c_m is a modest constant depending only on the dimension m and $\kappa(\cdot)$ denotes the 2-norm condition number of a rectangular matrix. Equation (3.2) tells us that when X is highly ill-conditioned, the QR factorization may be extremely sensitive to perturbations. When we compute an orthonormal basis \hat{Q} in floating point arithmetic, we are not guaranteed accuracy much better than $\|\hat{Q} - Q\| \leq c_m \kappa(X)u$ (at least, as long as the columns of X do not vary significantly in magnitude).

Because the rational filter amplifies the v_1 component in each column of Q_0 by $1/d$ in (2.1), X_1 is usually extremely ill-conditioned. Intuitively, $\kappa(X_1)$ cannot be much worse than $|r(\lambda_1)|/|r(\lambda_m)|$ and not much better than $|r(\lambda_1)|/|r(\lambda_2)|$ because v_1 is present in each column with magnitude near $|r(\lambda_1)|$ while the rest of the target eigenpairs are present with magnitude at least $|r(\lambda_m)|$ and no greater than $|r(\lambda_2)|$. Proposition 3.1 makes this intuition precise in the form of an upper bound and asymptotic lower bound. The implication is that the error in the computed orthonormal

basis \hat{Q}_1 is on the order of u/d as long as the columns of Q_0 are not orthogonal to the dangerous eigenvector, as we observed in [Figure 3.2](#).

PROPOSITION 3.1 (Dangerous eigenvalues). *Let $A \in \mathbb{C}^{n \times n}$ and $r : \Lambda \rightarrow \mathbb{C}$ satisfy [\(1.3\)](#) and [\(1.4\)](#), respectively, and given orthonormal $Q_0 \in \mathbb{C}^{n \times m}$, let $X_1 = r(A)Q_0$. If $V_1^*Q_0$ has full rank, then the condition number of X_1 satisfies*

$$(3.3) \quad \frac{\|v_1^*Q_0\|}{d|r(\lambda_2)|} + \mathcal{O}(1) \leq \kappa(X_1) \leq \left| \frac{r(\lambda_1)}{r(\lambda_m)} \right| \|(V_1^*Q_0)^{-1}\|, \quad \text{as } d \rightarrow 0.$$

Proof. The condition number of X_1 may be written as $\kappa(X_1) = \sigma_1(X_1)/\sigma_m(X_1)$, where $\sigma_1(X_1) \geq \dots \geq \sigma_m(X_1)$ are the singular values of X_1 . To bound $\sigma_1(X_1)$ above, we substitute the spectral decomposition $r(A) = Vr(\Lambda)V^*$ into the definition of X_1 and estimate $\sigma_1(X_1) \leq |r(\Lambda_1)|\|V^*Q_0\| \leq |r(\lambda_1)|$. To bound $\sigma_m(X_1)$ below, we use the spectral decomposition in [\(1.3\)](#) to write

$$(3.4) \quad X_1 = [V_1 \quad V_2] \begin{bmatrix} M_1 \\ M_2 \end{bmatrix},$$

where $M_1 = r(\Lambda_1)V_1^*Q_0$ and $M_2 = r(\Lambda_2)V_2^*Q_0$. Because V is unitary, the singular values of X_1 are precisely those of the right-most matrix. Furthermore, $\sigma_m(X_1) \geq \sigma_m(M_1)$ since adding rows can only increase the singular values of a matrix. Finally, since $\sigma_m(M_1) = \|M_1^{-1}\|^{-1}$, we have that $\kappa(X_1) \leq \sigma_1(X_1)\|M_1^{-1}\|$. We estimate that

$$\|M_1^{-1}\| = \|(V_1^*Q_0)^{-1}r(\Lambda_1)^{-1}\| \leq \|(V_1^*Q_0)^{-1}\| |r(\lambda_m)|^{-1}.$$

Collecting the bounds on $\sigma_1(X_1)$ and $\|M_1^{-1}\|$ establishes the upper bound in [\(3.3\)](#).

To establish the asymptotic lower bound, we apply [\(3.1\)](#) to $r(A)Q_0$, obtaining

$$(3.5) \quad X_1 = \sum_{i=1}^n r(\lambda_i)v_i v_i^* Q_0 = \frac{v_1^* Q_0}{d} v_1 + \mathcal{O}(1), \quad \text{as } d \rightarrow 0.$$

Taking norms provides an asymptotic lower bound on $\sigma_1(X_1)$. To obtain a lower bound on $\sigma_m(X_1)^{-1}$, we can bound $\sigma_m(X_1)$ from above with an interlacing property for singular values of matrices subject to rank one perturbations. We rewrite [\(3.5\)](#) as

$$X_1 = r(\lambda_1)v_1 v_1^* Q_0 + V \text{diag}(0, r(\lambda_2), \dots, r(\lambda_n))V^* Q_0 = N_1 + N_2.$$

Now, $\sigma_2(N_1) = 0$ and $\sigma_1(N_2) \leq |r(\lambda_2)|$ so, by interlacing [\[15\]](#), we obtain the estimate

$$\sigma_2(X_1) \leq \sigma_1(N_2) + \sigma_2(N_1) \leq |r(\lambda_2)|.$$

As $\sigma_m(X_1) \leq \sigma_2(X_1)$ implies that $1/\sigma_m(X_1) \geq |r(\lambda_2)|^{-1}$, collecting lower bounds concludes the proof of [\(3.3\)](#). \square

The factor $\|(V_1^*Q_0)^{-1}\|$ in [Proposition 3.1](#) appears naturally in connection with subspace iteration, and we will encounter it again in [section 5](#). It is precisely the reciprocal of $\cos \theta_1(\mathcal{S}_k, \mathcal{V})$ (see [Definition 2.2](#)), approaching unity when \mathcal{V} and \mathcal{S}_0 are nearby and blowing up quadratically when they are made orthogonal. In [Proposition 3.1](#) it indicates that X_1 may suffer additional ill-conditioning if the initial subspace \mathcal{S}_0 is accidentally chosen to be too near orthogonal to \mathcal{V} .⁴

⁴When Q_0 is selected so that its entries are independent, identically distributed Gaussian random variables, $\|(V_1^*Q_0)^{-1}\|$ is roughly \sqrt{m} in expectation, but may be an order of magnitude or so larger with nontrivial probability. A powerful workaround is to work with a slightly larger subspace and take m larger than the number of target eigenvalues; this dramatically reduces the probability of large $\|(V_1^*Q_0)^{-1}\|$ [\[3\]](#).

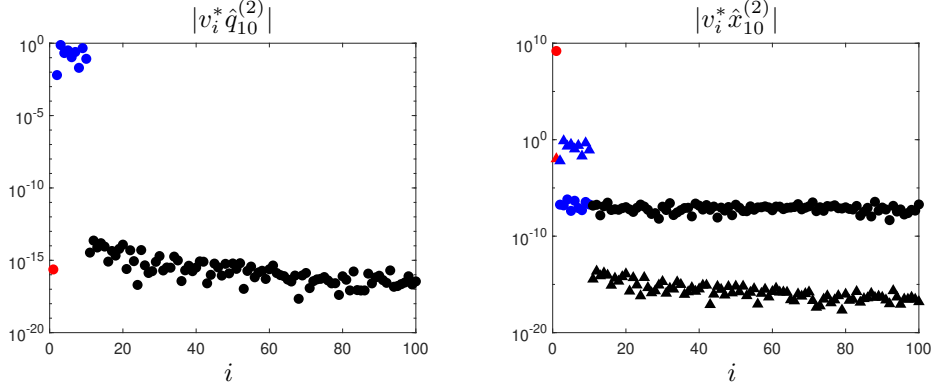


FIGURE 4.1. The structure of the iterates \hat{X}_2 and \hat{Q}_2 after a second iteration of subspace iteration with a rational filter. On the left, the eigenvector coordinates of the 10th column of the computed orthonormal basis color coded for dangerous component (red), remaining target components (blue), and unwanted components (black). On the right, the eigenvector coordinates of the 1st (circles) and 10th (triangles) columns of the computed basis \hat{X}_2 with the same color code used in the left panel.

4. Twice is enough. In Proposition 3.1, the asymptotic lower bound in (3.3) plummets if the columns of Q_0 are taken nearly orthogonal to v_1 , the dangerous eigenvector. Intuitively, this is because the rational filter has nothing to amplify when v_1 is absent in the columns of Q_0 . If v_1 is present with magnitude no greater than $\mathcal{O}(d)$ in Q_0 , then the columns of X_1 are not strongly aligned along any single eigenvector and the conditioning of X_1 is likely to improve. Crucially, this intuition holds even if v_1 dominates in one column but not the others. The main point is that the columns of X_1 are no longer necessarily close to a linearly dependent set.

Let's return to the example of Figure 3.1. If we print out the residual norms of the target eigenpairs after the second iteration of (2.1), we see remarkable improvement:

6.7997e-15	2.5942e-14	2.268e-13	4.3433e-14	9.1978e-14
1.3716e-14	9.7045e-14	3.4121e-14	1.4594e-13	4.0235e-14

Now all the target pairs have been resolved to within 13 or 14 digits of accuracy, in contrast to Figure 3.2 (left). If we examine the computed orthonormal basis used to extract the Ritz pairs, we observe that the noise in the direction of the unwanted eigenvectors has also been reduced to the order of u , compared with u/d in the first iteration. Figure 4.1 (left) illustrates the composition of the 10th column of \hat{Q}_2 , which is representative of the last $m - 1$ columns.

The reason for the restored accuracy in the computed orthonormal basis is that, unlike X_1 , the basis X_2 has an even blend of the target eigenvector directions in all but the first of its columns. Figure 4.1 (right) displays the magnitude of the eigenvector coordinates for the first (circular markers) and last (triangular markers) columns of the computed basis, \hat{X}_2 . In the first column, the dangerous direction is effectively the only direction present, since all other components appear with relative magnitude near u , while the last column of \hat{X}_2 contains order one components in each target direction with the unwanted directions completely filtered out. The remaining columns of \hat{X}_2 are similar in composition to the last. Without v_1 dominating in every column, we are able to accurately extract an orthonormal basis.

The clue to the stark difference in the composition of \hat{X}_1 and \hat{X}_2 is contained in Figure 3.2. There, we see that the first column of \hat{Q}_1 is dominated by the dangerous eigenvector, up to the 9th or 10th digit. Consequently, the remaining columns of \hat{Q}_1 are nearly orthogonal to v_1 . We observe this in Figure 3.2 (right), where

$v_1^* q_1^{(1)} \approx 10^{-11}$. When the rational filter is applied to \hat{Q}_1 in the second iteration, the amplification of v_1 restores an even blend of the target eigenvectors in the last $m - 1$ columns of \hat{X}_2 , rather than boosting v_1 above the others.

4.1. A well-conditioned basis. Motivated by the preceding discussion, we now examine the condition number of the second iterate, X_2 , when $q_1^{(1)}$ is a good approximation to v_1 and, consequently, *all but one* of the columns of Q_1 are deficient in the dangerous direction. We then explain why the deficiency of v_1 in the actual computed orthonormal basis \hat{Q}_1 occurs in just the right proportion to disarm the dangerous eigenvalue.

To investigate how a weak presence of v_1 in columns of Q_1 improves the conditioning of X_2 , we break the target eigenvector coordinates of Q_1 into blocks, as

$$(4.1) \quad V_1^* Q_1 = \begin{bmatrix} v_1^* q_1^{(1)} & v_1^* \tilde{Q}_1 \\ \tilde{V}_1^* q_1^{(1)} & \tilde{V}_1^* \tilde{Q}_1 \end{bmatrix} = \begin{bmatrix} a & b \\ c & D \end{bmatrix}.$$

Here, we use \tilde{V}_1 and \tilde{Q}_1 to denote the $n \times (m - 1)$ matrices formed by removing the first columns of V_1 and Q_1 , respectively. When $q_1^{(1)}$ closely approximates v_1 , then $\|c\|$ is small due to the orthogonality of the eigenvectors. Moreover, $\|b\|$ is also small because the columns of \tilde{Q}_1 are nearly orthogonal to v_1 . Let us suppose that $q_1^{(1)} = v_1 + \mathcal{O}(d)$, so that b and c are $\mathcal{O}(d)$ (we explain why this holds momentarily, following [Theorem 4.1](#)).

After applying the rational filter to Q_1 , the eigenvector coordinates $V_1^* X_2$ inherit a natural block structure from (4.1). Letting $\tilde{\Lambda}_1 = \text{diag}(\lambda_2, \dots, \lambda_m)$, we have that

$$(4.2) \quad V_1^* X_2 = r(\Lambda_1) V_1^* Q_1 = \begin{bmatrix} r(\lambda_1) a & r(\lambda_1) b \\ r(\tilde{\Lambda}_1) c & r(\tilde{\Lambda}_1) D \end{bmatrix}.$$

While the bottom left block remains small, with norm no greater than $|r(\lambda_2)|\|c\| = \mathcal{O}(d)$, the entire first row is amplified by $|r(\lambda_1)|$ so that $\|r(\lambda_1)b\| \approx \|b\|/d$.

To estimate the condition number of X_2 , we scale the columns of X_2 with the $m \times m$ diagonal matrix

$$(4.3) \quad T = \text{diag}(r(\lambda_1)^{-1}, 1, \dots, 1)$$

This diagonal scaling does not alter $\text{span}(X_2)$ or the sensitivity of the orthonormal basis, $Q_2 = \text{qf}(X_2)$. (Note that scaling the columns of X_1 has no effect in [Proposition 3.1](#), as the columns of X_1 all have magnitude $\approx 1/d$.) However, it conveniently puts the diagonal blocks in (4.2) on equal footing and ensures that $\sigma_1(X_2 T) = \mathcal{O}(1)$, so that any ill-conditioning due to the dangerous eigenvalue is captured in the smallest singular value of $X_2 T$. This allows us to focus on computing a lower bound for $\sigma_m(X_2 T)$ or, equivalently, an upper bound for $1/\sigma_m(X_2 T)$. Just as in the proof of [Proposition 3.1](#), it suffices to bound $\|(V_1^* X_2 T)^{-1}\|$ from above (assuming as usual that $V_1^* Q_1$, and therefore $V_1^* X_2$, has full rank).

With all of the ingredients in place, the estimate is fairly straightforward. After the column scaling, $V_1^* X_2 T$ is approximately block upper triangular. We have that

$$(4.4) \quad V_1^* X_2 T = \begin{bmatrix} r(\lambda_1) a & r(\lambda_1) b \\ r(\tilde{\Lambda}_1) c & r(\tilde{\Lambda}_1) D \end{bmatrix} T = \begin{bmatrix} a & b/d \\ r(\tilde{\Lambda}_1) c & r(\tilde{\Lambda}_1) D \end{bmatrix} + \mathcal{O}(d).$$

We can apply the formula for 2×2 block upper triangular matrix inversion and the fact that matrix inversion is locally Lipschitz continuous to compute (for d sufficiently

small)

$$(4.5) \quad (V_1^* X_2 T)^{-1} = \begin{bmatrix} a^{-1} & -a^{-1} D^{-1} r(\tilde{\Lambda}_1)^{-1} b/d \\ & D^{-1} r(\tilde{\Lambda}_1)^{-1} \end{bmatrix} (I + \mathcal{O}(d)).$$

The norm of the block upper triangular matrix in (4.5) is bounded by the sum of the norms of the blocks, so we conclude that $1/\sigma_m(X_2 T) \leq \|(V_1^* X_2 T)^{-1}\| = \mathcal{O}(1)$ when $\|b\| = \mathcal{O}(d)$. Estimating the norms of these blocks individually and combining with an estimate for $\sigma_1(X_2 T)$ leads to the following upper bound on $\kappa(X_2 T)$.

THEOREM 4.1 (Twice-is-enough). *Let $A \in \mathbb{C}^{n \times n}$ and $r : \Lambda \rightarrow \mathbb{C}$ satisfy (1.3) and (1.4), respectively, and given orthonormal $Q_1 \in \mathbb{C}^{n \times m}$, let $X_2 = r(A)Q_1$. Let b and D denote the blocks of $V_1^* Q_1$ in (4.1) and let $T = \text{diag}(r(\lambda_1)^{-1}, 1, \dots, 1) \in \mathbb{C}^{m \times m}$. If D is invertible and the first column of Q_1 satisfies $\|q_1^{(1)} - v_1\| = \mathcal{O}(d)$, then $\|b\| = \mathcal{O}(d)$ and*

$$(4.6) \quad \kappa(X_2 T) \leq M \left(\left(\frac{\|b\|}{d} + 1 \right) \frac{\|D^{-1}\|}{|r(\lambda_m)|} + 1 \right) + \mathcal{O}(d) \quad \text{as} \quad d \rightarrow 0.$$

Here, $M = \|b\|/d + \max\{1, |r(\lambda_2)|\}$.

Proof. First, the hypothesis $\|q_1^{(1)} - v_1\| = \mathcal{O}(d)$ immediately implies that $\|a\| = 1 + \mathcal{O}(d)$ and $\|b\| = \mathcal{O}(d)$. Then, following the discussion above, it suffices to bound $\|X_2 T\|$ and the norms of the blocks in (4.5). The condition number of $X_2 T$ is bounded above by the product of these two estimates. Since $\|r(\tilde{\Lambda}_1)^{-1}\| = |r(\lambda_m)|^{-1}$, we obtain that

$$(4.7) \quad 1/\sigma_m(X_2 T) \leq \|V_1^* X_2 T\| \leq 1 + \frac{\|D^{-1}\|}{|r(\lambda_m)|} \left(1 + \frac{\|b\|}{d} \right) + \mathcal{O}(d).$$

On the other hand, we can write $V^* X_2 T$ in block form analogous to (4.4), as

$$X_2 T = \begin{bmatrix} a & \tilde{b}/d \\ & r(\tilde{\Lambda}) \tilde{D} \end{bmatrix} + \mathcal{O}(d),$$

where $\tilde{b} = V^* q_1^{(1)}$ and $\tilde{D} = V^* \tilde{Q}_1$. Calculating the norm of the block diagonal component and the off-diagonal component separately and applying the triangle inequality yields $\|X_2 T\| \leq M$. Collecting with the bound in (4.7) concludes the proof. \square

Theorem 4.1 tells us that X_2 is only a simple column scaling away from a well-conditioned basis when the first column of Q_1 approximates v_1 with accuracy $\mathcal{O}(d)$. Since the sensitivity (and numerical computation) of the QR factorization is not effected by column scaling, the $\mathcal{O}(1)$ bound on $\kappa(X_2 T)$ in (4.6) explains why the computed orthonormal basis for \mathcal{S}_2 is accurate to unit round-off. This line of analysis follows naturally from our observation about the eigenvector coordinates of \hat{Q}_1 in Figure 3.2 (right), but one question remains that is worth briefly addressing. Why is the first column of the computed orthonormal basis, \hat{Q}_1 , such a good approximation to v_1 ?

The answer is that $\hat{q}_1^{(1)}$ is essentially the first column of X_1 after normalization, up to the unit round-off u . In particular, it is unaffected by the u/d errors in \hat{Q}_1 caused by ill-conditioning in X_1 (see Proposition 3.1). These errors are concentrated in the later columns of \hat{Q}_1 because of the nested structure of Householder reflections (or Givens

rotations) used to make X_1 upper triangular. We have that $x_1/\|x_1\| = v_1 + \mathcal{O}(d)$ by (3.1), so we expect that $\hat{q}_1^{(1)} = v_1 + \mathcal{O}(d)$ also, as observed in Figure 3.2.

Finally, if the orthogonal factor is computed with modified Gram-Schmidt instead of Householder reflections or Givens rotations, the columns of \hat{Q}_1 lose orthogonality in proportion to the condition number of the ill-conditioned basis X_1 . The consequence of this is that the block $v_1^*(\hat{Q}_1)_{(2:m)}$ from (4.1) may be as large as u/d instead of $\mathcal{O}(d)$, even though $\hat{q}_1^{(1)} = v_1 + \mathcal{O}(d)$. This may alter the order of magnitude of $\kappa(X_2 T)$ when $d \ll \sqrt{u}$ (since then, $u/d \gg d$) as the balance in Theorem 4.1 is disrupted. In particular, twice may no longer be enough to eradicate the dangerous eigenvalue-related ill-conditioning in \hat{X}_2 . A similar effect is observed for non-normal matrices in section 6 even when Householder reflections or Givens rotations are employed in the QR factorizations.

5. Convergence and stability. So far, our analysis of dangerous eigenvalues has focused on the conditioning of the iterates X_1, X_2, \dots in (2.1) and the corresponding accuracy in the computed orthonormal bases. Indeed, this perspective explains the u/d errors observed in the first iteration (see Figure 3.2) and provides the essential insight into the restored accuracy observed in the second iteration (see Figure 4.1). But we have not yet explained how the round-off errors incurred while applying the ill-conditioned rational filter enter the picture. Nor have we discussed how these round-off errors, together with the error in the computed orthonormal basis, accumulate during the iterations in (2.1).

To apply the rational filter $r(A)$ to an $n \times m$ matrix Q in practice, one solves linear systems with a shift at each pole and takes a weighted average of the solutions:

$$(5.1) \quad r(A)Q = \sum_{j=1}^{\ell} \omega_j X^{(j)}, \quad \text{where} \quad (z_j I - A)X^{(j)} = Q, \quad j = 1, \dots, \ell.$$

If the linear systems are solved with a backward stable algorithm, then the computed solutions $\hat{X}^{(j)}$ satisfy, for each $j = 1, \dots, \ell$,

$$(5.2) \quad (z_j I - A - \mathcal{E}_j)\hat{X}^{(j)} = Q, \quad \|\mathcal{E}_j\| \leq \gamma \|A\| u.$$

Here, \mathcal{E}_j is the backward error and γ is a constant, with modest dependence on z_1, \dots, z_ℓ and the dimension of Q , such that $\gamma u \ll 1$ for typical situations.⁵

Now, if we neglect errors made while forming the linear combination on the left-hand side of (5.1), then the forward error in $r(A)Q$ can be written as⁶

$$(5.3) \quad \hat{X} - r(A)Q = \sum_{k=1}^{\ell} \omega_k (z_k I - A)^{-1} \mathcal{E}_k \hat{X}^{(k)}, \quad \text{where} \quad \hat{X} = \sum_{k=1}^{\ell} \omega_k \hat{X}^{(k)}.$$

Due to the appearance of \mathcal{E}_j , the terms in the left-hand sum are all on the order of u except for the term corresponding to the pole near the dangerous eigenvalue,

⁵This characterization can be modified to accommodate inexact solution techniques, such as iterative methods, but γ may be much larger, depending on the stability properties of the particular numerical method [12, p. 339].

⁶For clarity in exposition, we neglect the round-off errors accrued when forming the linear combination in the right-hand side of (5.1) in order to focus on the effects of the ill-conditioned linear system. For typical choices of the weights and nodes defining $r(A)$, this amounts to discarding a term on the order of u .

whose index we call $j = j_*$. In the dangerous term, $(z_{j_*} I - A)^{-1}$ amplifies the v_1 components in the columns of \mathcal{E}_{j_*} by a factor of $1/d$. Similarly, the components of v_1 in the columns of Q are amplified to order $1/d$ in the corresponding columns of $\hat{X}^{(j_*)}$ (this is made precise by expanding (5.2) in a Neumann series). Therefore, the relative errors in the columns of \hat{X} are on the order of u/d .

Thus, every time $r(A)$ is applied in (2.1), relative errors of order u/d are accrued in the columns of \hat{X}_k . On the one hand, our understanding of accuracy in the computed orthonormal basis \hat{Q}_k (developed in [sections 3](#) and [4](#)) remains intact, because perturbations of relative order u/d to the columns of X_k have little effect on the leading-order estimates for $\kappa(X_k)$. On the other hand, we may wonder: what effect do such perturbations have on $\text{span}(X_k)$ and the geometric convergence implied in [Theorem 2.1](#)?

Recent analyses of subspace iteration accelerated with a rational filter suggest that $\text{span}(\hat{X}_k)$ tends to \mathcal{V} geometrically at roughly the expected rate until a threshold of accuracy is reached, at which point convergence plateaus [\[14\]](#). This threshold is usually the same order of magnitude as the error accrued in the subspace at each iteration, i.e., in the columns of \hat{X}_k . Similar results have been derived for perturbations in the entries of the matrix $r(A)$ (this work does not consider filters explicitly) [\[10\]](#). However, the evidence of the experiments in [Figures 1.1](#) and [1.2](#) and in [section 4](#) indicates that errors in $\text{span}(\hat{X}_k)$ caused by dangerous eigenvalues do not prevent the Rayleigh–Ritz procedure from finding vectors in $\text{span}(\hat{X}_k)$ that approximate the target eigenvectors to unit round-off accuracy. We now show that errors in \hat{X}_k caused by the dangerous eigenvalue do not lead to early stagnation or instability in the computed iterates. In the worst case, they may slow the geometric convergence rate by a factor of roughly $(1 - u/d)^{-1}$. Moreover, the iteration is stable as long as the columns of the initial guess Q_0 are not too near to \mathcal{V}^\perp (see [Figure 5.1](#)).

5.1. One-step refinement bounds. The amplifying power of the dangerous eigenvalue leads to large relative errors in the columns of \hat{X}_k . However, the errors possess an important quality: the amplification is entirely in the direction of v_1 so that the relative errors in the unwanted direction are still small. To understand how these structured perturbations influence $\hat{\mathcal{S}}_k = \text{span}(\hat{X}_k)$, we gather the errors accrued during the k th iteration into a perturbation to the orthonormal basis for $\hat{\mathcal{S}}_{k-1}$ and construct a one-step refinement bound as in [Theorem 2.3](#). Formulated precisely, we replace (2.1) with the perturbed form

$$(5.4) \quad \hat{X}_k = r(A)(Q'_{k-1} + R_k), \quad Q'_k = \text{qf}(\hat{X}_k).$$

Note that we include any errors in the computed orthonormal factor in R_k , placing the emphasis on $\hat{\mathcal{S}}_k = \text{span}(\hat{X}_k) = \text{span}(Q'_k)$ rather than on $\text{span}(\hat{Q}_k)$. This causes no difficulty since, as we know from [section 4](#), the error $\hat{Q}_k - Q'_k$ is on the order of u for $k \geq 2$. Since Q'_k is an orthonormal basis, $\hat{\mathcal{S}}_k$ and $\text{span}(Q'_k)$ only differ by a term not much larger than u .

To begin, we establish the form (5.4) by way of the residuals of the linear systems in (5.3) and study the structure of R_k . To measure the columns of R_k relative to the columns of \hat{X}_k , it is convenient to apply the diagonal scaling

$$(5.5) \quad C_k = \text{diag}(\|(\hat{X}_k)_1\|, \dots, \|(\hat{X}_k)_m\|)/\sqrt{m},$$

so that $\|\hat{X}_k C_k\| \leq 1$. We also need the majorization of the rational filter, denoted

$$(5.6) \quad \tilde{r}(\lambda) = \sum_{j=1}^{\ell} |\omega_j| |(z_j - \lambda)^{-1}|.$$

As usual, $\tilde{r}(\Lambda_1)$ and $\tilde{r}(\Lambda_2)$ are the matrices when the function in (5.6) is applied to the diagonal matrices Λ_1 and Λ_2 . Observe that $\tilde{r}(\Lambda_1)r(\Lambda_1)^{-1} = \mathcal{O}(1)$ as $d \rightarrow 0$, because the poles near the dangerous eigenvalue cancel.

LEMMA 5.1. *Let $A \in \mathbb{C}^{n \times n}$ and $r : \Lambda \rightarrow \mathbb{C}$ satisfy (1.3) and (1.4), respectively. Given $Q \in \mathbb{C}^{n \times m}$, let $\hat{X} = \sum_{j=1}^{\ell} \omega_j \hat{X}^{(j)}$ with each $\hat{X}^{(j)}$ satisfying (5.2). Then, there is an $R \in \mathbb{C}^{n \times m}$ such that $\hat{X} = r(A)(Q + R)$ and*

$$(5.7) \quad \|P_V R\| \leq \gamma_1 \|A\| u/d \quad \text{and} \quad \|(I - P_V)r(A)RC\| \leq \gamma_2 \|A\| u.$$

Here, $\gamma_1 = \gamma \|r(\Lambda_1)^{-1} \tilde{r}(\Lambda_1)\|$, $\gamma_2 = \gamma \|\tilde{r}(\Lambda_2)\|$, and C is the diagonal scaling in (5.5) (with index k suppressed).

Proof. Because each $\hat{X}^{(j)}$ satisfies (5.2) and $\hat{X} = \sum_{j=1}^{\ell} \omega_j \hat{X}^{(j)}$, we collect like terms in (5.3) and compute

$$(5.8) \quad \hat{X} = r(A)Q + \sum_{j=1}^{\ell} \omega_j (z_j I - A)^{-1} R^{(j)},$$

where $R^{(j)} = \mathcal{E}^{(j)} \hat{X}$. Note that $\|R^{(j)} C\| \leq \gamma \|A\| u$, for $j = 1, \dots, \ell$, by (5.2).

We compute R directly by comparing (5.8) with $\hat{X} = r(A)(Q + R)$ and noting that we need $r(A)R = \sum_{j=1}^{\ell} \omega_j (z_j I - A)^{-1} R^{(j)}$. Inserting the eigenvalue decomposition $A = V\Lambda V^*$ into both sides and inverting $r(A) = Vr(\Lambda)V^*$, we obtain

$$(5.9) \quad R = Vr(\Lambda)^{-1} \left(\sum_{j=1}^{\ell} \omega_j (z_j I - \Lambda)^{-1} V^* R^{(j)} \right).$$

Calculating $P_V R$ and $(I - P_V)r(A)RC$ directly from (5.9) and applying the backward error bounds in (5.2) to bound the residuals $\|R^{(j)}\|$ uniformly, we obtain the bounds in (5.7). \square

Lemma 5.1 demonstrates that the perturbations R_k in (5.4) capture the essential structure of the errors in \hat{X}_k . First, R_k perturbs Q'_{k-1} with relative magnitude u/d and direction in the subspace \mathcal{V} . Second, R_k perturbs the columns of X_k with relative magnitude u and direction in the subspace \mathcal{V}^\perp . We note that $\|V_2^* R_k C_k\|$ itself is not small when the filter is very good, i.e., close to unit-round off on the unwanted eigenvalues, as $\|r(\Lambda_2)^{-1} \tilde{r}(\Lambda_2)\|$ may be extremely large. However, the forward application of the filter cancels any large factors in $r(\Lambda_2)^{-1}$ exactly.

With Lemma 5.1 in hand, we can calculate a one-step refinement bound generalizing Theorem 2.3 to the perturbed iteration in (5.4). While the u/d relative errors in \hat{X}_k are felt in the refinement factor in (5.10), they do not appear in the additive perturbation to $\tan \theta_1(\hat{\mathcal{S}}_k, \mathcal{V})$. This point is crucial because, as we show in subsection 5.2, the size of the additive term determines the threshold for stagnation in a worst case accumulation of errors.

THEOREM 5.2. *Let $A \in \mathbb{C}^{n \times n}$ and $r : \Lambda \rightarrow \mathbb{C}$ satisfy (1.3) and (1.4), respectively, and let $\hat{\mathcal{S}}_k = \text{span}(\hat{X}_k)$, with \hat{X}_k defined in (5.4) and R_k satisfying (5.7). If $\cos \theta_1(\hat{\mathcal{S}}_{k-1}, \mathcal{V}) \geq \gamma_1 \|A\|u/d$, then*

$$(5.10) \quad \tan \theta_1(\hat{\mathcal{S}}_k, \mathcal{V}) \leq \left| \frac{r(\lambda_{m+1})}{r(\lambda_m)} \right| \frac{\tan \theta_1(\hat{\mathcal{S}}_{k-1}, \mathcal{V})}{1 - \alpha_k} + \beta_k,$$

where $\alpha_k \leq \gamma_1 \|A\|u/(d \cos \theta_1(\hat{\mathcal{S}}_{k-1}, \mathcal{V}))$ and $\beta_k \leq \gamma_2 \|A\| \kappa(\hat{X}_k C_k) u$.

Proof. Calculating directly as in the proof of [Theorem 2.3](#), we selectively expand $T(\hat{X}_k, V_1) = (I - P_{\mathcal{V}})\hat{X}_k C_k (V_1^* \hat{X}_k C_k)^{-1}$ using the definition of \hat{X}_k :

$$(5.11) \quad \begin{aligned} T(\hat{X}_k, V_1) &= r(A)(I - P_{\mathcal{V}})Q'_{k-1} C_k (r(\Lambda_1)V_1^*(Q'_{k-1} + R_k)C_k)^{-1} \\ &\quad + r(A)(I - P_{\mathcal{V}})R_k C_k (V_1^* \hat{X}_k C_k)^{-1}. \end{aligned}$$

Applying the bound on $\|(I - P_{\mathcal{V}})r(A)R_k C_k\|$ from [Lemma 5.1](#), we bound the norm of the term on the second line by β_k , because $r(A)(I - P_{\mathcal{V}}) = (I - P_{\mathcal{V}})r(A)$ and $\|(V_1^* \hat{X}_k C_k)^{-1}\| \leq \kappa(\hat{X}_k C_k)$ (since $\|\hat{X}_k C_k\| \leq 1$ and V_1 has orthonormal columns). To bound the right-hand side on the first line, we employ a Neumann series and factor out $(V_1^* Q'_{k-1})^{-1}$ in the inverse of the perturbed term, i.e.,

$$(V_1^*(Q'_{k-1} + R_k))^{-1} = (V_1^* Q'_{k-1})^{-1} (I + \sum_{k=1}^{\infty} (V_1^* Q'_{k-1})^{-k+1} (V_1^* R_k)^k (V_1^* Q'_{k-1})^{-1}).$$

Since $T(Q'_{k-1}, V_1) = (I - P_{\mathcal{V}})Q'_{k-1}(V_1^* Q'_{k-1})^{-1}$, we substitute the series back into the right-hand side of the first line (and note that the diagonal matrices in the first line cancel) to obtain

$$(5.12) \quad r(A)T(Q'_{k-1}, V_1)(I + \sum_{k=1}^{\infty} (V_1^* Q'_{k-1})^{-k+1} (V_1^* R_k)^k (V_1^* Q'_{k-1})^{-1} r(\Lambda_1)^{-1}.$$

Taking norms and applying the bound for $\|P_{\mathcal{V}}R_k\| = \|V_1^* R_k\|$ from [Lemma 5.1](#) along with the identity $\|(V_1^* Q'_{k-1})^{-1}\| = 1/\cos \theta_1(\hat{\mathcal{S}}_k, \mathcal{V})$ from [Definition 2.2](#), we bound the expression in (5.12) by

$$\|r(\Lambda_2)\| \|r(\Lambda_1)^{-1}\| \frac{\tan \theta_1(\hat{\mathcal{S}}_{k-1}, \mathcal{V})}{1 - \alpha_k}.$$

Noting that $\|r(\Lambda_2)\| = |r(\lambda_{m+1})|$, $\|r(\Lambda_1)^{-1}\| = |r(\lambda_m)|^{-1}$, and collecting the bounds for the two lines in (5.11) establishes (5.10). \square

The significance of [Theorem 5.2](#) is that the errors in \hat{X}_k that lie in the target subspace, \mathcal{V} , only impact the geometric convergence rate, but do not contribute to the “inhomogeneous” term β_k in (5.10).⁷ This worst case scenario occurs over one iteration only when the perturbations are aligned so as to maximally cancel the components of \mathcal{V} present in the basis Q'_{k-1} . In fact, such errors are just as likely to align perfectly with the \mathcal{V} components of Q'_{k-1} and improve the convergence rate by $(1 - \alpha_k)$, so the impact on the geometric convergence rate implied by (5.10) is probably not observed in practice.

⁷We use the term inhomogeneous here in anticipation of the recurrence relation, derived from (5.10), that is used for stability analysis in [subsection 5.2](#).

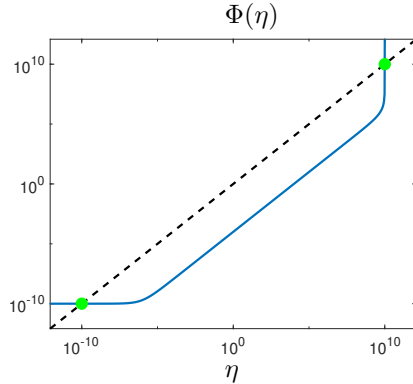


FIGURE 5.1. The dynamics of perturbed subspace iteration from (5.14). The solid line is the graph of $\Phi(\eta)$ and its fixed points (green circles) are marked at the intersections where $\Phi(\eta) = \eta$. If $\tan \theta_1(\hat{\mathcal{S}}_0, \mathcal{V})$ falls between the two fixed points (green circles), then the $\tan \theta_1(\hat{\mathcal{S}}_k, \mathcal{V})$ must converge geometrically to a threshold near the lower fixed point (see Theorem 5.4).

On the other hand, the errors in \hat{X}_k that lie in \mathcal{V}^\perp degrade the expected refinement through the inhomogeneous term β_k and, due to orthogonality, have a tangible effect on the convergence of subspace iteration in floating point arithmetic. Note that, in harmony with sections 3 and 4, the magnitude of β_k is proportional to the condition number of the basis \hat{X}_k after column scaling. Thus, we expect $\beta_1 \approx u/d$, but that $\beta_k \approx u$ for $k \geq 2$.

5.2. Stability and stagnation. According to Theorem 5.2, the refinement in the search subspace at each iteration is approximately geometric with rate comparable to Theorem 2.1, up to the size of the errors β_k introduced in \mathcal{V}^\perp at each iteration. As we accumulate iterations, the errors in \mathcal{V}^\perp are filtered out by the application of $r(A)$ to \hat{X}_k and, in the apt words of the authors of [14], “the dominant error term is the one most recently introduced.” As the sequence β_k remains roughly stable at the order of u after the first iteration, we expect that $\hat{\mathcal{S}}_k$ converges geometrically toward \mathcal{V} until a threshold of about u is reached, after which convergence stagnates. This is exactly what we observe in Figures 1.1 and 1.2.

However, it is worth noting that the rate of convergence in Theorem 5.2 depends on $\cos \theta_1(\hat{\mathcal{S}}_{k-1}, \mathcal{V})$. Typically, the α_k terms are on the order of u/d . But when $\hat{\mathcal{S}}_{k-1}$ is nearly orthogonal to \mathcal{V} , the factor $(1 - \alpha_k)$ in (5.10) may be very small and the one-step refinement bound may not imply any refinement in $\hat{\mathcal{S}}_k$ at all. With a slight change of perspective, we now characterize the long term behavior of the iterates in (5.4) and address questions of both stability and the threshold for stagnation in subspace refinement.

Let us introduce the constants $\rho = |r(\lambda_{m+1})|/|r(\lambda_m)|$, $\epsilon_1 = \gamma_1 \|A\| u/d$, and $\epsilon_2 = \gamma_2 \|A\| \hat{M} u$, where \hat{M} is an $\mathcal{O}(1)$ uniform bound on $\kappa(X_k C_k)$ (i.e., from Theorem 4.1). Consider the function

$$(5.13) \quad \Phi(\eta) = \frac{\rho \eta}{1 - \epsilon_1(1 + \eta)} + \epsilon_2.$$

Because $1/\cos \theta \leq 1 + \tan \theta$ when $0 \leq \theta \leq \pi/2$, Theorem 5.2 implies that for all $k \geq 2$, we have $\tan \theta_1(\hat{\mathcal{S}}_k, \mathcal{V}) \leq \Phi(\tan \theta_1(\hat{\mathcal{S}}_{k-1}, \mathcal{V}))$. We can understand the “worst-case” behavior of subspace iteration by studying the discrete dynamics of $\tan \theta_1(\hat{\mathcal{S}}_0, \mathcal{V})$, for some initial subspace $\hat{\mathcal{S}}_0$, under the map Φ .

Given $\eta_0 > 0$, let $\phi_k(\eta_0)$ denote the k -fold iteration of the map Φ on the point η_0 , so that (letting $f \circ g$ denote the composition of two functions) we have

$$(5.14) \quad \phi_k(\eta_0) = \underbrace{\Phi \circ \cdots \circ \Phi}_{k}(\eta_0).$$

We call η_* a fixed point of Φ if $\Phi(\eta_*) = \eta_*$ and say that η_* is monotone attracting for $\Omega \subset [0, \infty)$ if $\phi_k(\eta) \rightarrow \eta_*$ monotonically as $k \rightarrow \infty$ for all $\eta \in \Omega$. After applying Φ to $\tan \theta_1(\hat{\mathcal{S}}_0, \mathcal{V})$ k times, we see that

$$(5.15) \quad \tan \theta_1(\hat{\mathcal{S}}_k, \mathcal{V}) \leq \phi_k \left(\tan \theta_1(\hat{\mathcal{S}}_0, \mathcal{V}) \right).$$

Consequently, the fixed points of Φ and their attracting sets provide insight into the behavior of $\tan \theta_1(\hat{\mathcal{S}}_k, \mathcal{V})$ in the limit $k \rightarrow \infty$, in particular, about the convergence and stability of the iteration in (5.4).

LEMMA 5.3. *Define the map $\Phi : [0, \infty) \rightarrow [0, \infty)$ as in (5.13), with constants $\rho > 0$ and $\epsilon_1, \epsilon_2 \geq 0$. Let*

$$\delta = (1 - \rho - \epsilon_1(1 - \epsilon_2)) / (2\epsilon_1), \quad \text{and} \quad \sigma = \epsilon_2(1 - \epsilon_1).$$

If $\delta^2 > \sigma$, then Φ has precisely two fixed points, given by $\eta_{\pm} = \delta \pm \sqrt{\delta^2 - \sigma}$. Moreover, the fixed point η_- is monotone attracting on $[0, \eta_+]$.

Proof. Starting from the fixed point equation $\Phi(\eta_*) = \eta_*$, we multiply through by $1 - \epsilon_1(1 + \eta_*)$ to obtain the quadratic equation

$$(5.16) \quad \epsilon_1 \eta_*^2 - [1 - \rho - \epsilon_1(1 - \epsilon_2)]\eta_* + \epsilon_2(1 - \epsilon_1) = 0.$$

Applying the quadratic formula for the roots and rewriting in terms of δ and σ concludes the calculation. Now, the quadratic on the left-hand side of (5.16) is negative between the roots, which implies that $\Phi(\eta) > 0$ for $0 < \eta < \eta_-$ and $\Phi(\eta) < 0$ for $\eta_- < \eta < \eta_+$. The change of sign at each fixed point implies that η_- attracts nearby points and that η_+ repels nearby points. Because Φ is non-decreasing and has no other fixed points, we conclude that η_- is monotone attracting on $[0, \eta_+]$. \square

Lemma 5.3 shows that if $\tan \theta_1(\hat{\mathcal{S}}_0, \mathcal{V}) < \eta_+$, then $\tan \theta_1(\hat{\mathcal{S}}_k, \mathcal{V})$ must eventually be on the order of η_- or better for all sufficiently large k . Recalling that the constants ϵ_1 and ϵ_2 are on the order of u/d and u , respectively, and that ρ is the filtered spectral ratio, we estimate the size of the fixed points to leading order as

$$(5.17) \quad \eta_- \approx \frac{\epsilon_2}{1 - \rho}, \quad \text{and} \quad \eta_+ \approx \frac{1 - \alpha}{\epsilon_1}.$$

Crucially, the lower fixed point η_- is on the order of u , not u/d . Having established stability properties of the perturbed iteration in (5.4), we can now estimate the rate of convergence to the fixed point η_- .

THEOREM 5.4. *Define the map $\Phi : [0, \infty) \rightarrow [0, \infty)$ as in (5.13), with constants $\rho > 0$ and $\epsilon_1, \epsilon_2 \geq 0$. Given $0 \leq \eta_0 < \eta_+$, let ϕ_k denote the k -fold iteration of Φ as in (5.14). If Φ satisfies the hypotheses of Lemma 5.3, then*

$$(5.18) \quad \phi_k(\eta_0) \leq \left(\frac{\rho}{1 - \epsilon_1(1 + \eta_0)} \right)^k \eta_0 + \frac{\epsilon_2}{1 - \rho(1 - \epsilon_1(1 + \eta_0))^{-1}}.$$

Proof. Denote $\eta_k = \phi_k(\eta_0)$, for $k \geq 1$. By hypothesis, [Lemma 5.3](#) applies, so $\eta_k \rightarrow \eta_-$ monotonically as $k \rightarrow \infty$. In particular, $\eta_k \leq \eta_0$ for each k . Combining this uniform bound with the definitions of η_k above and Φ in [\(5.13\)](#), we have the upper bound

$$(5.19) \quad \eta_k = \Phi(\eta_k - 1) \leq \frac{\rho \eta_{k-1}}{1 - \epsilon_1(1 + \eta_0)} + \epsilon_2, \quad k \geq 1.$$

Letting $\tilde{\rho} = \rho/(1 - \epsilon_1(1 + \eta_0))$, we iterate the bound in [\(5.19\)](#) $k - 1$ times to obtain

$$\eta_k \leq \tilde{\rho}^k \eta_0 + \epsilon_2 \sum_{j=0}^{k-1} \tilde{\rho}^j \leq \tilde{\rho}^k \eta_0 + \epsilon_2/(1 - \tilde{\rho}).$$

Plugging the original parameters back into the constant $\tilde{\rho}$ establishes [\(5.18\)](#). \square

Thus, [Theorem 5.4](#) and [\(5.15\)](#) demonstrate that the reduction of $\tan \theta_1(\hat{\mathcal{S}}_k, \mathcal{V})$ down to the order of η_- is approximately geometric with rate close to ρ . So (accounting for the fact that the additive perturbation term is actually on the order of u/d in the first iteration) it takes approximately $1 + \log(\eta_-)/\log(\rho)$ steps for $\hat{\mathcal{S}}_k$ to converge to within order u of \mathcal{V} , as measured by the tangent of the principle angle between the two subspaces.

6. Non-normal matrices. We now consider the case of an $n \times n$ diagonalizable matrix A whose eigenvectors are not orthogonal. Although a straightforward extension of [Proposition 3.1](#) shows that the condition number of X_1 still scales, generically, like $1/d$ (see [Proposition 6.1](#) below), the effect of a dangerous eigenvalue on subsequent iterates, X_2, X_3, \dots , computed via [\(2.1\)](#) is distinct in the non-normal case due to interactions among non-orthogonal modes. In fact, the condition numbers of the computed iterates do not improve during subsequent iterations unless approximate eigenvectors (i.e., from Ritz vectors) are incorporated into the subspace iteration (see [Algorithm 6.1](#)). Even with this modification, the condition numbers may remain large after one iteration when d is very small (loosely, when $d \ll \sqrt{u}$), unlike the normal case. Here, we demonstrate that $\kappa(X_k)$ is typically reduced in step with the error in the Ritz vectors and that $\kappa(X_k) \approx (u/d)^k$ in the best case (i.e., when $|r(\lambda_{m+1})|/|r(\lambda_m)| \approx u$ and the Ritz vectors are well-conditioned at each iteration).

When A does not have an orthogonal basis of eigenvectors (but is still diagonalizable), the orthogonal spectral projectors $v_i v_i^*$ that diagonalize the filter in [\(3.1\)](#) are replaced by oblique spectral projectors, so that

$$(6.1) \quad r(A)x = \sum_{i=1}^n r(\lambda_i) \frac{w_i^* x}{w_i^* v_i} v_i = \frac{w_1^* x}{d(w_1^* v_1)} v_1 + \mathcal{O}(1), \quad \text{as } d \rightarrow 0.$$

Here, w_1, \dots, w_n are the left eigenvectors of A , satisfying $w_i^* A = \lambda_i w_i^*$ with $\|w_i\| = 1$ for $i = 1, \dots, n$. Likewise, the spectral decomposition in [\(1.3\)](#) is replaced by

$$(6.2) \quad A = V_1 \Lambda_1 W_1^* + V_1 \Lambda_2 W_2^*,$$

where the i th column of $W = [W_1 \ W_2]$ is $(w_i^* v_i)^{-1} w_i$. With this normalization, V and W form a biorthogonal system, meaning that $W^* V = I$, I being the $n \times n$ identity matrix. In the biorthogonal system, the dangerous eigenvalue amplifies the w_1 component in the input x along the v_1 direction in the output $r(A)x$. Due to biorthogonality, v_1 and w_1 are parallel only when v_1 is orthogonal to v_2, \dots, v_n .

6.1. First iteration. To develop a sense of how non-normality impacts the conditioning of the iterates, it's worthwhile to revisit the analysis of $\kappa(X_1)$ in [Proposition 3.1](#) when A is only diagonalizable. While the condition number of X_1 is still $\mathcal{O}(1/d)$ as $d \rightarrow 0$, the constants in the bound now depend on the structure of the left and right eigenvectors. This is because the stretching and shrinking actions of A no longer belong solely to its eigenvalues, but can be enhanced or attenuated by interactions among non-orthogonal eigenvectors. We denote the smallest singular values of V_1 and W_1 by $\sigma_m(V_1)$ and $\sigma_m(W_1)$, respectively.

PROPOSITION 6.1 (Dangerous eigenvalues of non-normal matrices). *Let diagonalizable $A \in \mathbb{C}^{n \times n}$ and $r : \Lambda \rightarrow \mathbb{C}$ satisfy (6.1) and (6.2), respectively, and given orthonormal $Q_0 \in \mathbb{C}^{n \times m}$, let $X_1 = r(A)Q_0$. If $U_1 = \text{qf}(W_1)$ and $U_1^*Q_0$ has full rank, then the condition number of X satisfies*

$$(6.3) \quad \frac{\|w_1^*Q_0\|/|w_1^*v_1|}{d\kappa(V)|r(\lambda_2)|} + \mathcal{O}(1) \leq \kappa(X_1) \leq \left| \frac{r(\lambda_1)}{r(\lambda_m)} \right| \frac{\kappa(V)\|(U_1^*Q_0)^{-1}\|}{\sigma_m(V_1)\sigma_m(W_1)}, \quad \text{as } d \rightarrow 0.$$

Proof. The steps of the proof are essentially identical to those in [Proposition 3.1](#) if (6.1) and (6.2) are used in place of (1.3) and (3.1), so we emphasize the adaptations made for non-orthogonal eigenvectors. For the largest singular value of X_1 , we bound $\sigma_1(X_1) = \|r(A)Q_0\| \leq \kappa(V)|r(\lambda_1)|$, since $|r(\lambda_1)| \leq \|r(A)\| \leq \kappa(V)\|r(\Lambda)\|$ in the non-normal case. If we use (6.2) to decompose X_1 as in (3.4), the singular values of $r(A)W_1^*Q_0$ do not tell us directly about the singular values of X_1 because V is not unitary. However, if $\Omega_1R_1 = V_1$ and $\Omega_2R_2 = V_2$ are economy-sized QR factorizations, we can decompose

$$r(A)Q_0 = [\Omega_1 \quad \Omega_2] \begin{bmatrix} R_1r(\Lambda_1)W_1^*Q_0 \\ R_2r(\Lambda_2)W_2^*Q_0 \end{bmatrix}.$$

Since Ω_1 and Ω_2 have orthonormal columns, we apply the argument in the proof of [Proposition 3.1](#) to obtain the bound $1/\sigma_m(X_1) \leq \|(R_1r(\Lambda_1)W_1^*Q_0)^{-1}\|$. Now, R_1 has the same singular values as V_1 and $\|R_1^{-1}\| = 1/\sigma_m(R_1)$, so we have that

$$(6.4) \quad \kappa(X_1) \leq \frac{|r(\lambda_1)|}{|r(\lambda_m)|} \frac{\kappa(V)\|(W_1^*Q_0)^{-1}\|}{\sigma_m(V_1)}.$$

The upper bound in (6.3) follows by substituting the QR decomposition $U_1S_1 = W_1$ into (6.4) and noting that $\|S_1^{-1}\| = 1/\sigma_m(W_1)$.

A lower bound on $\sigma_1(X_1)$ follows directly from (6.1), analogous to (3.5). For the lower bound on $1/\sigma_m(X_1)$, we can use (6.1) to write X_1 as a rank one perturbation of the matrix

$$\tilde{N}_2 = V \text{diag}(0, \lambda_2, \dots, \lambda_m) W^* Q_0.$$

We have that $\sigma_1(N_2) \leq \|V\| \|W^*\| |r(\lambda_2)| = \kappa(V) |r(\lambda_2)|$, where the equality is due to biorthogonality, which implies that $W^* = V^{-1}$. By interlacing, we find that $1/\sigma_m(X_1) \geq 1/(\kappa(V) |r(\lambda_2)|)$, establishing the asymptotic lower bound in (6.3). \square

When A is normal, [Proposition 6.1](#) reduces to [Proposition 3.1](#). In the non-normal case, ill-conditioning in the eigenvectors, reflected in $\kappa(V)$, widens the interval between the upper and lower bounds. Similarly, ill-conditioning in the target eigenvectors, captured by the smallest singular values of V_1 and W_1 (since the columns of both matrices have unit norm), may widen the gap further. On the other hand, the dangerous eigenvalue itself is ill-conditioned when $|w_1^*v_1|$ is small.⁸ The left-hand side

⁸With $\|v_i\| = \|w_i\| = 1$, the quantity $|w_i^*v_i|^{-1}$ is Wilkinson's condition number for λ_i , measuring the first order sensitivity of the eigenvalue to infinitesimal perturbations in A .

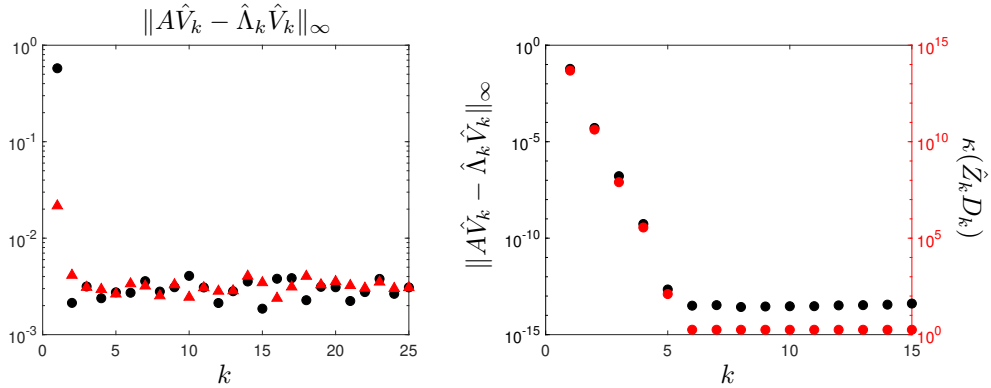


FIGURE 6.1. Dangerous eigenvalues of a non-normal matrix. The eigenvalues and rational filter are identical to the setup displayed in Figure 3.1, however, this matrix has non-orthogonal eigenvectors and the dangerous eigenvalue has been moved to distance $d = 10^{-13}$ from the pole at $z = 10$. On the left, the maximum residual of 10 target eigenpairs after each iteration of (2.1) (black circles) and a modified subspace iteration based on Schur vectors (red triangles). On the right, the maximum residuals of the target eigenpairs computed after each iteration of Algorithm 6.1 (black circles, left axis). The condition number of the iterates $\hat{Z}_k D_k$ (D_k scales the columns of \hat{Z}_k to have unit norm) decreases in step with the residuals, at a rate of about u/d per iteration (red circles, right axis).

of (6.3) illustrates how this may enhance the amplifying effects of the dangerous eigenvalue, increasing the asymptotic lower bound to $d|w_1^* v_1|^{-1}$. Broadly speaking, the widening gap between upper and lower bounds indicates that our picture is blurred in the non-normal case because the structure of the eigenvectors plays a key role. The extent of the damage may depend on where the ill-conditioning in V is concentrated.

6.2. Iterating with orthonormal bases. Now that we have a taste for the interaction between non-normality and dangerous eigenvalues in the initial iteration, we are ready to examine subsequent iterations. As in section 4, we focus on the coordinates of Q_1 in the eigenvector basis, partitioned into blocks as

$$(6.5) \quad W_1^* Q_1 = \begin{bmatrix} w_1^* q_1^{(1)} & w_1^* \tilde{Q}_1 \\ \tilde{W}_1^* q_1^{(1)} & \tilde{W}_1^* \tilde{Q}_1 \end{bmatrix}.$$

The critical observation about (6.5) is that, in contrast to the normal case, the upper right block is not small. Although the columns of \tilde{Q}_1 are still nearly orthogonal to v_1 , the eigenvectors v_1 and w_1 are only parallel in the special case that v_1 is orthogonal to v_2, \dots, v_n . Consequently, $w_1^* \tilde{Q}_1$ is typically $\mathcal{O}(1)$ and, when we compute $X_2 = r(A)Q_1$, the components in each column of Q_1 in the w_1 direction will be amplified according to (6.1). Each column of X_2 will be dominated by v_1 at magnitude $\mathcal{O}(1/d)$ and we are in the same ill-conditioned state as we were in the first iteration! This line of thinking seems to indicate that, when $r(A)$ is repeatedly applied to an orthonormal basis, subspace iteration for non-normal matrices must stagnate at an accuracy of $\approx u/d$ due to ill-conditioning in the iterates X_1, X_2, \dots

To illustrate, we return to the experimental setup illustrated in (3.1). We select the same rational filter and a matrix with the same eigenvalues, but now the eigenvector matrix is not orthogonal. The condition number of the eigenvector matrix is $\approx 10^2$, but the target eigenvectors themselves are not far from orthogonal. Figure 6.1 shows the maximum residual of the computed target eigenpairs after each of the first 10 iterations of (2.1). We also compare with a modified subspace iteration based on

Algorithm 6.1 Filtered subspace iteration with Rayleigh–Ritz projection.

Input: Given $A \in \mathbb{C}^{n \times n}$, $r : \Lambda \rightarrow \mathbb{C}$, and $Y_0 \in \mathbb{C}^{n \times m}$.

- 1: **for** $k = 1, 2, \dots$ **do**
- 2: Apply the filter $Z_k = r(A)Y_{k-1}$.
- 3: Compute orthonormal basis $Q_k = \text{qf}(Z_k)$.
- 4: Form $A_k = Q_k^* A Q_k$ and solve $A_k U_k = U_k \Theta_k$ for U_k, Θ_k .
- 5: Set $Y_k = Q_k U_k$.
- 6: **end for**

Output: Approximate eigenvalue matrix Θ_k and eigenvector matrix Y_k .

Schur vectors that is commonly used to compute eigenvalues of non-normal matrices. Both iterations apply the rational filter directly to an orthonormal basis for the search space and we see that the residuals stagnate at around u/d in both cases.

6.3. Iterating with approximate eigenvectors. So, what can we do to improve the conditioning of the iterates and the accuracy in the target eigenpairs? Consider another common variant of subspace iteration shown in [Algorithm 6.1](#), which forms the iterates Z_1, Z_2, \dots by applying $r(A)$ to approximate eigenvectors constructed from the Ritz vectors at each iteration. Let us partition $W_1^* Y_1$ in the usual way,

$$(6.6) \quad W_1^* Y_1 = \begin{bmatrix} w_1^* y_1^{(1)} & w_1^* \tilde{Y}_1 \\ \tilde{W}_1^* y_1^{(1)} & \tilde{W}_1^* \tilde{Y}_1 \end{bmatrix} = \begin{bmatrix} e & f \\ g & H \end{bmatrix},$$

where \tilde{Y}_1 and \tilde{Q}_1 denote the last $m - 1$ columns of W_1 and Q_1 , respectively. Now, because the left and right eigenvectors are biorthogonal, w_1^* annihilates the remaining target eigenvectors v_2, \dots, v_m , so the upper right block f in (6.6) is small when the columns of Y_1 are a good approximation to the target eigenvectors. In turn, small $\|f\|$ mitigates the amplification of v_1 in the last $m - 1$ columns of Z_2 .

Unfortunately, the behavior of approximate eigenvectors computed with (6.1) may vary widely for general non-normal matrices. In exact arithmetic, their accuracy will depend not only on the quality of the rational filter (the eigenvalues of $r(A)$), but on interactions among non-orthogonal eigenvectors. This can delay convergence and may lead to instability on a computer. In floating point arithmetic, it is further limited by the accuracy in the computed orthonormal basis and Ritz vectors. In spite of these difficulties, we can glean some practical insight into a distinguished feature of the non-normal setting by examining a “best-case” situation.

Let us suppose that the non-normal effects are relatively mild, that $r(\cdot)$ filters out the unwanted eigenvalues to unit round-off or better (as in [3.1](#)), and that the Ritz vectors are computed accurately at each iteration. In this regime, the accuracy of the approximate eigenvectors Y_1 is limited mainly by the accuracy in the computed orthonormal basis, \tilde{Q}_1 , and we can focus on the influence of the dangerous eigenvalue in the second iteration (and beyond). From our analysis of the first iteration in [subsection 6.1](#), we expect that $\|\hat{Q}_1 - Q_1\| \approx u/d$ and, therefore, (by our assumptions on the filter and the Ritz vectors) that $\|\tilde{Y}_1 - Y_1\| \approx u/d$.

Interestingly, the order of magnitude of block f in (6.6) is of distinctly different magnitude than the analogous block b in the normal case. Instead of the perfect balancing between b and $r(\lambda_1)$ when the filter is applied (leading to perfectly well-conditioned columns of X_2), we have the order-of-magnitude estimate $\|f\| |r(\lambda_1)| \approx$

u/d^2 . In other words, v_1 may still dominate each column of Z_2 when $d \ll \sqrt{u}$, but the gap in magnitude between the v_1 component and the remaining target components in the last $m-1$ columns is reduced by a factor of u/d at the second iteration. [Figure 6.1](#) illustrates this phenomena in action with the same matrix and rational filter used for the experiments in [subsection 6.2](#). The residuals in the target eigenpairs decrease geometrically from the first iteration with rate u/d , mirroring the reduction in the condition number of the iterates Z_k (after scaling the columns to unit norm).

Thus, for a mildly non-normal matrix with a dangerous eigenvalue at distance $d \ll \sqrt{u}$ from a pole of $r(\cdot)$, two iterations are not usually enough to remove the adverse influence of the dangerous eigenvalue. Instead the target residuals and the errors in the computed orthonormal basis are often refined in step down to the unit round-off (depending on the sensitivity of the target eigenpairs). As in the normal case, round-off errors caused by the dangerous eigenvalue may even go unnoticed when the rational filter is mediocre so that the noise in the unwanted directions is dominated by poor filtering.

7. Restarting Arnoldi. Now that we understand the right-hand side of [Figure 1.1](#), let us examine the stagnation of Arnoldi with shift-and-invert enhancement illustrated in the left-hand panel of the same figure. Unlike subspace iteration, which applies $r(A)$ iteratively to a subspace of fixed dimension, Arnoldi refines the subspace by expanding it. Given an initial unit vector $q_1 \in \mathbb{C}^n$, shift-and-invert Arnoldi computes the iterates

$$(7.1) \quad y_k = s(A)q_{k-1}, \quad q_k = \text{mgsr}(y_k; q_1, \dots, q_{k-1}),$$

with the expression $\text{mgsr}(\cdot)$ indicating that y_k is orthogonalized against q_1, \dots, q_{k-1} using modified Gram–Schmidt with full reorthogonalization [[12](#), pp.307-308].

After k steps of (7.1), we have an $n \times k$ orthonormal basis $Q_k = [q_1 \cdots q_k]$ and we can approximate eigenpairs of A in one of two ways:

- Directly from the eigenpairs of the upper Hessenberg matrix H_k generated from the weights calculated during modified Gram–Schmidt [[17](#), p.253].
- A Rayleigh–Ritz step by computing eigenpairs of $A_k = Q_k^* A Q_k$.

Usually, the upper Hessenberg matrix is the method of choice because it does not require any additional matrix–vector products. However, when a dangerous eigenvalue is present, the upper Hessenberg matrix in the Arnoldi decomposition of $s(A)$ typically has norm $\|H_k\| = \mathcal{O}(d)$: this makes accurate calculation of the remaining target eigenvalues challenging for standard dense solvers. To keep the focus on the accuracy in the computed basis Q_k , we work with A_k , but we revisit H_k at the end of this section.

In keeping with the analysis in [sections 3](#) and [4](#), we can understand the accuracy in the computed orthonormal basis \hat{Q}_k through the conditioning of the matrix

$$(7.2) \quad Y_k = [q_1 \cdots q_{k-1} \ y_k], \quad k = 2, 3, 4, \dots$$

The matrix Q_k from the Arnoldi iterations is precisely the QR factorization of Y_k obtained by orthogonalizing y_k against the previous $(k-1)$ columns, which are already an orthonormal set. If y_k is not too closely aligned with $\text{span}(q_1, \dots, q_{k-1})$, then the matrix Y_k is well-conditioned, at least after a simple column scaling. Consequently, $Q_k = \text{qf}(Y_k)$ is not too sensitive to perturbations caused by round-off in Y_k , as discussed in [subsection 3.1](#). However, if y_k is closely aligned with any of the previous columns, the smallest singular value of Y_k will be close to zero and Q_k will be very sensitive to round-off in Y_k .

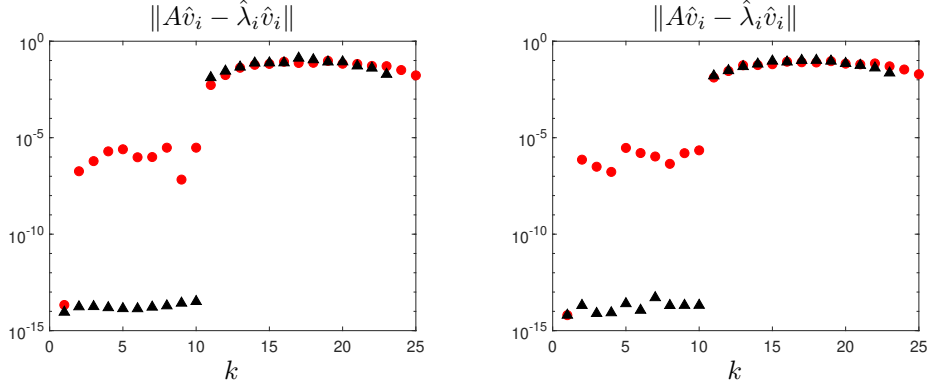


FIGURE 7.1. After restarting Arnoldi with Ritz vectors that are nearly orthogonal to the dangerous direction, Arnoldi produces approximations to the target eigenpairs with accuracy near the unit round-off. Both plots compare eigenpair residuals after 25 steps of shift-and-invert Arnoldi with no restart (red circles) to eigenpair residuals obtained after 25 total steps of shift-and-invert Arnoldi with the Ritz restart described in the text. The eigenpairs were extracted from $Q_{25}^*AQ_{25}$ in the left panel and from the Hessenberg matrix H_{25} in the right panel.

This perspective provides an explanation for the stagnation observed in Figure 1.1. When q_1 is chosen randomly, $v_1^*q_1$ is generically $\mathcal{O}(1)$ (as $d \rightarrow 0$). After applying the shift-and-invert filter, we calculate (as usual) that

$$y_2 = s(A)q_1 = \frac{v_1^*q_1}{d}v_1 + \mathcal{O}(1).$$

After we orthogonalize y_2 against q_1 to compute q_2 , then for some constant h_2 , we have

$$(7.3) \quad q_2 = h_2 \frac{v_1^*q_1}{d} (v_1 - (v_1^*q_1)q_1) + \mathcal{O}(1).$$

In other words, q_2 may not be dominated by v_1 , but $\text{span}(q_1, q_2)$ contains approximations to v_1 that are accurate to $\mathcal{O}(d)$.

Now, note that q_2 is not near orthogonal to v_1 unless q_1 happens to be very closely aligned with v_1 . This means that the subsequent iterate y_3 is also aligned with v_1 , and therefore with a vector in $\text{span}(q_1, q_2)$, to about order d . Consequently, the matrix Y_3 is ill conditioned and we expect that Q_3 , and in particular q_3 , can only be accurate to about order u/d when computed in floating point precision. Moreover, q_3 is not dominated by v_1 and this process repeats, so that each iterate y_k is closely aligned with v_1 in $\text{span}(q_1, q_2)$, leading to errors in q_k on the order of u/d .

In our discussion above, note that y_3 was only aligned with v_1 , and thus close to $\text{span}(q_1, q_2)$, because q_2 was not nearly orthogonal to v_1 . Unlike in subspace iteration, the dangerous direction is never rendered harmless by orthogonalizing directly against it! The geometric picture of the iterates y_2, y_3, y_4, \dots being attracted to v_1 as a result of q_2, q_3, q_4, \dots not being sufficiently orthogonal to v_1 suggests an interesting fix. If we restart the Arnoldi iteration with the Ritz approximation associated to v_1 after the second iteration, the picture changes drastically. Again, y_2 is aligned with v_1 , but now it is orthogonalized against $q_1 = v_1 + \mathcal{O}(d)$. The corresponding q_2 may not be particularly accurate, but this doesn't matter much: the point is that all subsequent iterates are orthogonalized against the dangerous direction (via q_1) up to order $\mathcal{O}(d)$. Analogous to the situation encountered in subspace iteration, the iterates

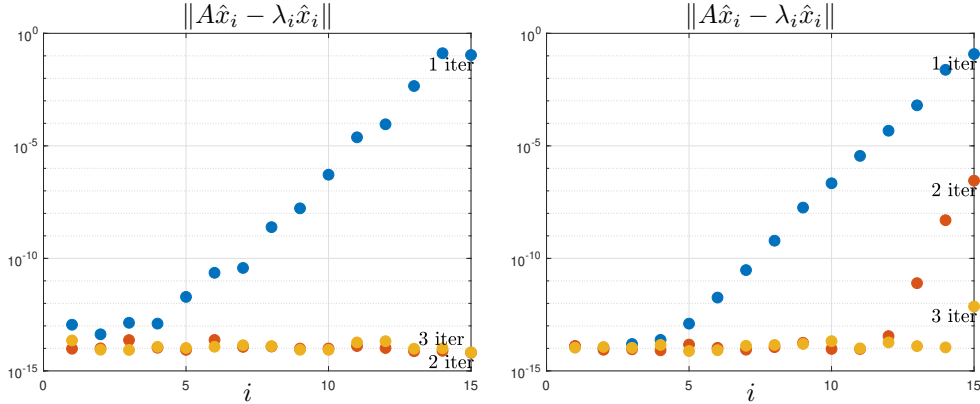


FIGURE 8.1. *Convergence with multiple dangerous eigenvalues.* Left: high-quality filter ($\ell = 32$ quadrature points); two iterations is enough, and increasing N further does not improve convergence. Right: medium-quality filter ($\ell = 8$). The convergence (after two iterations) reflects that of subspace iteration.

y_3, y_4, y_5, \dots , are no longer dominated by v_1 and, consequently, q_3, q_4, q_5, \dots can be computed perfectly accurately. In a sense, we are tricking Arnoldi into running in the orthogonal complement of the dangerous direction.

Figure 7.1 demonstrates this restart strategy in action. As we saw earlier, 25 iterations of shift-and-invert Arnoldi leads to stagnation in 9 of the 10 target eigenpairs. However, we can resolve all 10 target eigenpairs to unit round-off accuracy in 25 iterations if we restart with the Ritz vector corresponding to the dangerous direction after the second iteration. The right Ritz vector is easy to identify: it is the one most closely aligned with the second iteration y_2 . It's worth noting that the Ritz restart strategy seems to be equally successful when eigenpairs are extracted from the Hessenberg matrix H_k instead of $Q_k^* A Q_k$ (see the right panel in Figure 7.1).

8. Multiple dangerous eigenvalues. For simplicity, our analysis has focused on the case where there is just one dangerous eigenvalue. However, other situations may arise more naturally in practice. When eigenvalues are heavily clustered, many dangerous eigenvalues may surround a single pole at a variety of distances. The main message of our results largely carry over to these cases. To illustrate this, we generate an 200×200 symmetric matrix with 15 target eigenvalues in $[10, 15]$, and we put a circular contour centered at 12.5. There are two dangerous eigenvalues at $10 + 10^{-13}$, and the other 13 target eigenvalues are clustered exponentially at the pole, taking the values $10 + 10^{-i}$, $i = 0, 1, 2, \dots, 12$. There are hence two dangerous eigenvalues, along with many less harmful but still dangerous eigenvalues. Figure 8.1 shows the results with two rational filters: one excellent and one medium quality. Just as in sections 3 and 4, we see that twice is enough if the filter quality is high; with a poorer filter, the iterates beyond the second behaves as if there was no dangerous eigenvalue (also, see the right panels in Figures 1.1 and 1.2).

Conclusions. Subspace and Arnoldi iterations can be extremely efficient and flexible tools for computing a few target eigenpairs when accelerated with a rational filter, but one must be cautious about eigenvalues clustering near the poles. The damage incurred by such dangerous eigenvalues is confined to the first iteration of subspace iteration: subsequent iterations self-correct and the eigenpairs are computed to machine precision as orthogonalization effectively deflates the dangerous direction. If the matrix is real-symmetric or, more generally, normal, then the influence of the dan-

gerous eigenvalue is corrected in just two iterations. For matrices whose eigenvectors are not orthogonal (or very near to orthogonal), self-correction occurs geometrically over a series of iterations at a rate of roughly u/d . For Arnoldi and similar Krylov schemes, we recommend restarting the iteration with the Ritz approximation to the dangerous eigenvector in order to resolve all target eigenpairs to full precision.

Acknowledgements. We would like to thank Alex Townsend for encouraging our investigation into the stability of contour integral eigensolvers and the dangers of eigenvalues located near quadrature nodes.

REFERENCES

- [1] A. P. Austin and L. N. Trefethen. Computing eigenvalues of real symmetric matrices with rational filters in real arithmetic. *SIAM J. Sci. Comp.*, 37(3):A1365–A1387, 2015.
- [2] A. Bjorck and G.H. Golub. Numerical methods for computing angles between linear subspaces. *Math. Comput.*, 27(123):579–594, 1973.
- [3] K. R. Davidson and S. J. Szarek. Local operator theory, random matrices and banach spaces. *Handbook of the geometry of Banach spaces*, 1(131):317–366, 2001.
- [4] S. Guttel, E. Polizzi, P. T. P. Tang, and G. Viaud. Zolotarev quadrature rules and load balancing for the FEAST eigensolver. *SIAM J. Sci. Comp.*, 37(4):A2100–A2122, 2015.
- [5] N. J. Higham. *Accuracy and stability of numerical algorithms*, volume 80. SIAM, 2002.
- [6] J. Kestyn, V. Kalantzis, E. Polizzi, and Y. Saad. PFEAST: a high performance sparse eigenvalue solver using distributed-memory linear solvers. In *SC'16: Proceedings of the International Conference for High Performance Computing, Networking, Storage and Analysis*, pages 178–189. IEEE, 2016.
- [7] B.N. Parlett. *The symmetric eigenvalue problem*. SIAM, 1998.
- [8] E. Polizzi. Density-matrix-based algorithm for solving eigenvalue problems. *Phys. Rev. B*, 79(11):115112, 2009.
- [9] Y. Saad. *Numerical methods for large eigenvalue problems: revised edition*. SIAM, 2011.
- [10] Y. Saad. Analysis of subspace iteration for eigenvalue problems with evolving matrices. *SIAM J. Matrix Anal. Appl.*, 37(1):103–122, 2016.
- [11] T. Sakurai and H. Sugiura. A projection method for generalized eigenvalue problems using numerical integration. *J. Comput. Appl. Math.*, 159(1):119–128, 2003.
- [12] G. W. Stewart. *Matrix Algorithms: Volume II: Eigensystems*. SIAM, 2001.
- [13] G. W. Stewart and J.-G. Sun. Matrix perturbation theory. 1990.
- [14] P. T. P. Tang and E. Polizzi. FEAST as a subspace iteration eigensolver accelerated by approximate spectral projection. *SIAM J. Matrix Anal. Appl.*, 35(2):354–390, 2014.
- [15] R. C. Thompson. The behavior of eigenvalues and singular values under perturbations of restricted rank. *Linear Algebra Appl.*, 13(1-2):69–78, 1976.
- [16] L. N. Trefethen and M. Embree. *Spectra and pseudospectra: the behavior of nonnormal matrices and operators*. Princeton University Press, 2005.
- [17] L.N. Trefethen and D. Bau III. *Numerical linear algebra*, volume 50. SIAM, 1997.
- [18] P. Zhu and A. V. Knyazev. Angles between subspaces and their tangents. *J. Numer. Math.*, 21(4):325–340, 2013.